Cover page

Exam information

NFYK10020E - Physics Thesis 60 ECTS, Niels Bohr Institute - Kontrakt:123256 (Kjartan Másson)

Handed in by

Kjartan Másson
bjv419@alumni.ku.dk

Exam administrators

Eksamensteam, tel 35 33 64 57
eksamen@science.ku.dk

Assessors

D. Jason Koskinen
Examiner
xdn365

Mauricio Bustamante
Examiner
Mbustamante@nbi.ku.dk
📞 +4535334778

Hand-in information

Titel: Secret interactions of ultra-high-energy cosmogenic neutrinos and their near-future discovery
Titel, engelsk: Secret interactions of ultra-high-energy cosmogenic neutrinos and their near-future discovery
Tro og love-erklæring: Yes
Indeholder besvarelsen fortroligt materiale: No

Secret Interactions of Ultra-High-Energy Cosmogenic Neutrinos and Their Near-Future Discovery
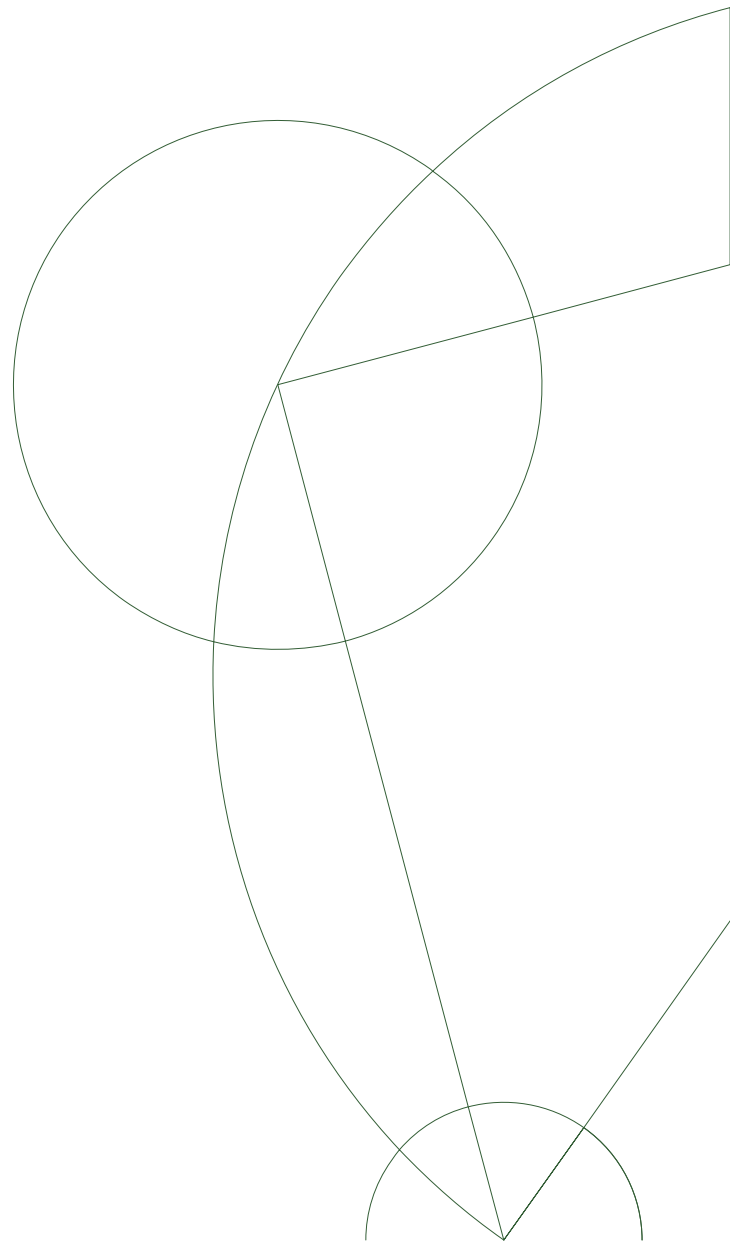
Kjartan Másson

Master's Thesis in Physics

Supervisor: Mauricio Bustamante

Niels Bohr Institute

University of Copenhagen

Date: August 16, 2021

ABSTRACT

Proposed stronger self-interactions of neutrinos beyond the Standard Model via a new mediator dubbed *secret neutrino interactions* (νSI) have been studied before as a candidate solution to major unresolved problems in physics. So far, there is no evidence for νSI with mediator masses up to ~ 100 MeV, yet they may still exist at higher masses. In order to probe them, we need *ultra-high-energy* (UHE) neutrinos, with energies in the EeV range, long-sought, but still undiscovered, on account of their tiny flux. Fortunately, the planned radio-antenna array of the IceCube-Gen2 detector will finally provide a realistic opportunity to discover UHE neutrinos, via the Askaryan radio emission that they should induce in the ice. This makes for an exciting opportunity to continue the search for νSI. We focus on UHE cosmogenic neutrinos, expected to be produced in the interaction of UHE cosmic rays (UHECRs) on cosmic photon backgrounds. We compute the effect of comosgenic neutrinos interacting with the low-energy relic neutrino background, via νSI, as they propagate to Earth. We forecast the the characteristic spectral features on the cosmogenic neutrino energy spectrum that are expected from νSI. We compute the associated expected number of detected events at IceCube-Gen2, accounting for the effect of neutrino attenuation inside the Earth and for the detector energy and angular resolution. At each stage of the calculation, we use state-of-the-art ingredients. With this, we lay our the groundwork for an end-to-end calculational framework to test νSI in IceCube-Gen2, and in other upcoming radio-detection neutrino telescopes.

ACKNOWLEDGMENTS

To my loving and supporting family

and

in the memory of Hans Bengtsson.

CONTENTS

CONTENTS

INTRODUCTION

Neutrinos are weakly interacting neutrally charged particles, which makes them great messengers for phenomena happening far beyond our own galaxy. Unlike other cosmic messengers such as photons and charged particles, neutrinos rarely scatter off surrounding matter and do not get deflected by magnetic fields. Thus neutrinos can carry untainted information across cosmological scales. Studying cosmic neutrinos allows us to investigate un-probed regions of our universe and explore possible new physics.

Currently there are a number of unsolved problems in physics that the Standard Model fails to explain. These include the origin of neutrino mass, the muon anomalous moment, tensions in cosmology, and the LSND anomaly; see chapter 2.4. New neutrino self-interactions beyond the Standard Model, dubbed *secret neutrino interactions* (νSI) have been proposed as possible solutions to these problems. νSI are proposed to occur via a new mediator, of undetermined mass and coupling strength. Their existence has been tested using in a variety of different ways, including using the measurements of the *cosmic microwave background* (CMB) [1–5], Big Bang nucleosynthesis [6–8], supernova neutrinos [9, 10], and laboratory measurements [11–14]. Recently high-energy (TeV–PeV) neutrinos of astrophysical origin were used to test νSI [15, 16]. The higher the neutrino energy used to probe νSI, the heavier the mediator mass that can be probed. No evidence for νSI has been found so far, for mediator masses up to $\sim$ 100 MeV.

Recent improvements in neutrino-detection technology, and more specifically the planned and current construction of a handful of Askaryan-based radio-telescopes such as IceCube-Gen2 will provide us, for the first time, with a realistic chance of discovering the long-predicted, but tiny flux of EeV-scale neutrinos. We focus on the theorized [17] but currently undetected flux of so-called cosmogenic neutrinos that are produced when *ultra-high-energy* (UHE) cosmic rays of $\gtrsim$ 10 EeV interact with CMB photons, producing neutrinos in the PeV– EeV range. If cosmogenic neutrinos undergo νSI, they may interact the cosmic background of low-energy relic neutrinos en route to Earth. νSI would induce characteristic spectral features in the energy spectrum of cosmogenic neutrinos. If the νSI mediator mass is in the range of 100 MeV–few GeV, then IceCube-Gen2 might have a chance of detecting the spectral features. This will be the topic of this thesis.

In chapter 2 we have a brief overview of the history of the neutrino discuss some of its basic properties. We then turn our attention to the specific model we use for νSI and talk about the production and propagation of cosmogenic neutrinos.

In chapter 3 we discuss the propagation of high-energy neutrinos, and how it is affected in the presence of νSI. We then apply the propagation equations to an injected flux of cosmogenic neutrinos computed using state-of-the-art software for ultra-high-energy-cosmic-ray propagation PRINCE. We compute how the flux of

cosmogenic neutrinos would look like and strategically vary the νSI parameters to observe changes in the predicted flux.

In chapter 4 we overview the current state of the IceCube detector and discuss the planned upgrades for IceCube-Gen2. We introduce Askaryan radiation as the basis for an upcoming new generation of radio-based neutrino telescopes. We how the possible in-Earth attenuation effects for a flux of cosmogenic neutrinos reaching IceCube-Gen2, and how we account for them using cutting edge neutrino-propagation software NuPropEarth. From there we make predictions for the number of detected neutrino events at IceCube-Gen2.

In chapter 5 we have a short discussion about our results, make conclusions, and discuss where we stand and where to move forward.

Throughout this thesis we make use of natural units $\hbar = c = 1$.

NEUTRINOS

2.1 WHAT ARE NEUTRINOS?

The discovery of a new weakly interacting particle can be traced back a to particular unsolved crisis in physics at the beginning of the 20th century. Observations of the radioactive decay of radium confirmed that the spectrum of produced β-particles was continuous, thus appearing to violate energy conservation [18]. In 1930 Wolfgang Pauli came up with a radical solution to the problem by proposing the existence of a neutrally charged undetected particle that he called the neutron that would later be renamed to the neutrino as it is known today. With the discovery of the neutron residing in atomic nuclei by James Chadwick in 1932, Wolfgang Pauli put it all together with his theory of the β-decay:

$$n \rightarrow p^+ + e^- + \bar{\nu}_e, \tag{2.1.1}$$

where inside of a radioactive nuclei the neutron n would decay into a positively charged proton p^+, emitting a negatively charged electron e^- and an anti-neutrino $\bar{\nu}_e$.

Today we have a better understanding of the properties and behaviour of neutrinos and have established that neutrinos only interact via the weak force mediated by W and Z bosons that is responsible for physical processes such as the β-decay mentioned above. Because the weak force is relatively feeble, the processes that are mediated solely by it are infrequent in Nature, making neutrinos extremely hard to detect.

A major unresolved problem in neutrino physics is the question of whether the neutrino is a Dirac or Majorana fermion. If the neutrino is Dirac then it has all of the same properties as other spin $1/2$ fermions such as the electron aside from the fact that it has no charge and therefore differs from its antiparticle by its helicity. In 1937 Ettore Majorana proposed the possibility that the neutrino might be its own antiparticle. As a result neutrinos could participate in certain forbidden interactions that violate lepton number conservation (the difference in the number of leptons and antileptons in elementary particle interactions). For years particle physicists have been trying to distinguish whether the neutrino is Dirac or Majorana by trying to observe the extremely rare neutrinoless double β-decay, where a β^+ and a β^- decay happens in an atomic nucleus simultaneously producing two virtual Majorana neutrinos that annihilate with each other.

The Homestake experiment conducted by Raymond Davis, Jr. and John N. Bahcall in the late 1960s, strove to confirm the mechanism of nuclear fusion within the core of our sun by capturing the excess produced neutrinos on Earth [19] [20]. The experiment itself was a success, however there was a resulting unexplainable mismatch in the number of captured neutrinos with the predicted amount by a

ratio of around 1/3. The discrepancy between the predicted and measured rates of neutrino detection was later found to be due to neutrino flavor oscillations. This discovery confirmed that neutrinos exist one of three flavor states ν_e, ν_μ and ν_τ and can oscillate between different flavor states over time.

2.2   NEUTRINO LANDSCAPE

We are exposed to a variety of neutrino fluxes coming from multiple sources. Figure 1 maps out the landscape of neutrino sources with their respective energies and travel distances en route to Earth. The main contributing sources of neutrinos that we know of include:

1. **Solar Neutrinos:** In nuclear fusion taking place in the cores of stars where hydrogen atoms fuse together to make helium, electron neutrinos are created as a side product:

$$p^+ + p^+ \;\;\rightarrow\;\; {}^2\text{H} + e^+ + \nu_e\,, \tag{2.2.1}$$
$$^2\text{H} + p^+ \;\;\rightarrow\;\; {}^3\text{He} + \gamma\,. \tag{2.2.2}$$
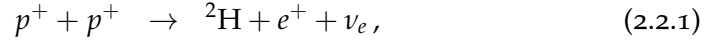
As opposed to photons produced during nuclear fusion that are constantly being absorbed and re-emitted by atoms before being able to escape the star, the neutrinos can pass through practically unaffected, thus carrying direct information about the internal processes happening inside the interior of stars. We are exposed to plenty of neutrinos on the surface of the Earth coming from our own Sun, where we are bombarded by a flux of solar neutrinos of about 6.5×10^{10} cm^{-3} s^{-1} with energies ranging from around 10^5–10^7 eV [22].

2. **Geoneutrinos:** Neutrinos are produced within the interior of the Earth in decay chains of radioactive isotopes, in particular uranium ^{238}U and thorium ^{232}Th. These are the lowest-energy neutrinos observed by present neutrino
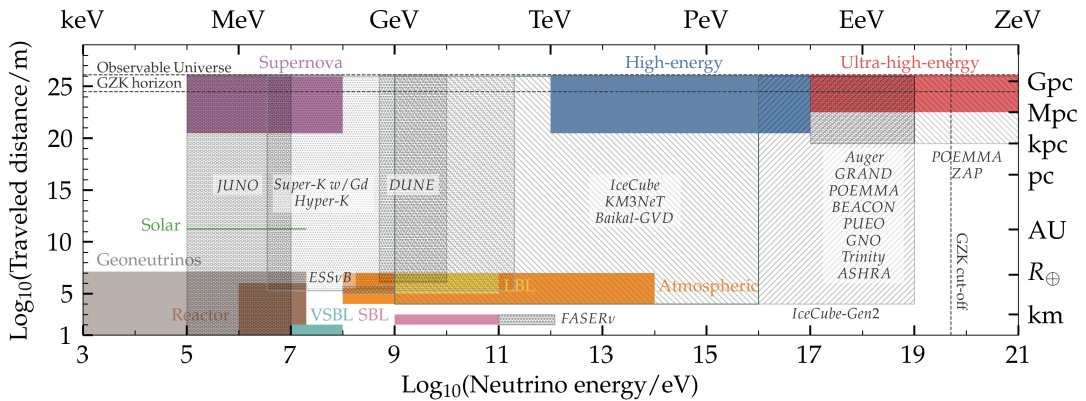

Figure 1: Current landscape of neutrinos that we are exposed to on the surface of the Earth. The colored regions show the energy ranges and traveled distance of neutrinos coming from specific sources. The shaded regions show the detection sensitivity of ongoing and upcoming neutrino detection experiments. Figure taken from [21].

detectors that can appear as a weak background in scintillator based neutrino experiments.

3. **Neutrinos from Nuclear Reactors:** Neutrinos are produced from β-decay of particles created from nuclear fission inside of nuclear reactors. In a general fission process 4.5% of the total energy goes into $\bar{\nu}_e$, thus producing a significant and steady flux of neutrinos with energies in the range of MeV.

4. **Atmospheric Neutrinos:** Cosmic rays can interact with protons and nuclei in the Earth's atmosphere creating a shower of particles, many of which are unstable and can produce neutrinos during their decay chains. Due to the wide spread in energy of the incoming cosmic rays on Earth atmospheric neutrinos have energies in the range of about 10^8–10^{14} eV.

5. **Neutrinos from Supernovae:** The very first observed extra-solar neutrino was from the SN1987A where a burst of neutrinos was detected in multiple observatories three hours before any visible light reached Earth. In supernovae cores, the high matter density leads to β-decay, photodisintegration, and electron capture, which result in a burst of MeV-scale neutrinos over a short timescale.

6. **Cosmic Neutrino Background CνB:** For the very first second after the Big Bang the Universe primarily consisted of electrons, positrons and neutrinos that were in thermal equilibrium maintained via the weak force. As the expansion rate of the Universe became larger than the rate of interaction of neutrinos with matter inside the primordial plasma, neutrinos decoupled from the rest of the matter. These neutrinos still exist today extremely cooled down by the cosmic expansion with an average neutrino energy of around 10^{-4}–10^{-6} eV per neutrino with a number density of 56 cm^{-3} for each neutrino flavor [23].

7. **Neutrinos from Particle Accelerators:** Neutrinos can be produced with particle accelerators. The standard technique involves hitting a target atomic nuclei with protons to produce unstable charged particles that are then accelerated through a tunnel. The charged products will pick up relativistic speeds before decaying, producing a directed neutrino beam. This kind of procedure allows for a very controlled environment of neutrino observations, making it valuable to study neutrino oscillations in particular.

8. **Astrophysical High-Energy and Ultra-High-Energy Neutrinos:** Neutrinos in the high (TeV – 10 PeV) and *ultra-high-energy* (UHE) (> 10 PeV) range produced from astrophysical sources or by the decay/interactions of cosmic rays from astrophysical sources. Their spectrum is still not very well understood, especially at the very high energies where charged particles cannot be confined within the magnetic fields of the Milky Way and thus believed to be of extra-galactic origin. Plausible source candidates include active galactic nuclei, gamma-ray-bursts, magnetars, and accretion shocks around cluster of galaxies [24].

9. **Cosmogenic Neutrinos:** These are the highest-energy steady sources of neutrinos that we know of today. Cosmogenic neutrinos are produced when

ultra-high energy cosmic ray interact with the CMB producing daughter particles that will decay into neutrinos with energies of around 10^{15}–10^{18} eV. These neutrinos will be the main scope of this thesis and are discussed more thoroughly in section 2.5.

2.3 NEUTRINO MIXING AND OSCILLATIONS

Neutrinos participate in weak interactions with other leptons as flavor states ν_e, ν_μ, ν_τ and their corresponding anti-particles $\bar{\nu}_e$, $\bar{\nu}_\mu$ and $\bar{\nu}_\tau$. Neutrinos are also known to oscillate between flavors while propagating, thus they must have a mass, as shown below. To explain neutrino oscillations, neutrinos exist in one of three different eigenstates of definite mass that we label as ν_1, ν_2 and ν_3. Thus we can consider any of the flavor states as superposition of a combination of mass states and vice versa. The mixing between flavor and mass states is described by the Pontecorvo–Maki–Nakagawa–Sakata (PMNS) matrix $\mathbf{U}$, where a change to either basis can performed as:

$$|\nu_k\rangle = \sum_\alpha U_{\alpha k} |\nu_\alpha\rangle, \quad |\nu_\alpha\rangle = \sum_k U_{\alpha k}^* |\nu_k\rangle . \qquad (2.3.1)$$

Where $i = 1, 2, 3$ and $\alpha = e, \mu, \tau$. Therefore a neutrino of a certain flavor is a superposition of neutrinos of the three mass eigeinstates, where $|U_{e1}|^2$ is for example the probability of a ν_e to be observed in mass eigenstate ν_1. Since both the mass and flavor states are orthogonal: $|\langle \nu_j|\nu_k\rangle|^2 = \delta_{jk}$ and $|\langle \nu_\alpha|\nu_\beta\rangle|^2 = \delta_{\alpha\beta}$, the PMNS matrix is unitary.

Since neutrinos are hard detect and measure, their masses have not been established. Measurements from cosmology have set an upper limit on the sum of the masses of neutrinos of $\sum m_\nu \lesssim 0.152$ eV [25], where detailed measurement of the CMB anisotropies reveal characteristics affected strongly by the density of relativistic massive neutrinos before photon decoupling epoch.

We also know the squared-mass differences $\Delta m_{ij}^2 \equiv m_i^2 - m_j^2$ of two independent sets of mass eigenstates from neutrino oscillation experiments. Observation of solar and atmospheric neutrinos resulted in a measured $\Delta m_{\text{SOL}}^2 \simeq 7.42 \times 10^{-5}$ eV^2 and $\Delta m_{\text{ATM}}^2 \simeq 2.5 \times 10^{-3}$ eV respectively [26] [27]. In the case of three-neutrino mixing there are three squared-mass differences but only two of them are independent since $\Delta m_{32}^2 + \Delta m_{21}^2 - \Delta m_{31}^2 = 0$. The labeling of the three different mass eigenstates are arbitrary and are just a matter of convention. The standard convention is to assign $\Delta m_{21}^2 \equiv \Delta m_{\text{SOL}}^2$ and since we only know the atmospheric squared difference up to an absolute value we consider two different scenarios of $\Delta m_{31}^2 \equiv |\Delta m_{\text{ATM}}^2|$ which we call normal ordering (NO) and $\Delta m_{32}^2 \equiv -|\Delta m_{\text{ATM}}^2|$ which we call inverted ordering (IO). Knowing the value of the lowest neutrino mass, we can compute the other neutrino masses for both scenarios as shown in Table 1.

Figure 2 shows the ranges of neutrino masses presently allowed by oscillation experiments and cosmology. In the case of NO we expect a mass difference of a few meV between the neutrinos, while for IO we see two neutrinos share very similar energies with a noticeably higher mass than the lightest neutrino.

Ordering	m_1	m_2	m_3
NO	m_1	$\sqrt{m_1^2 + \Delta m_{21}^2}$	$\sqrt{m_1^2 + \Delta m_{31}^2}$
IO	$\sqrt{m_3^2 - \Delta m_{32}^2 - \Delta m_{21}^2}$	$\sqrt{m_3^2 - \Delta m_{32}^2}$	m_3

Table 1: Neutrino masses as functions of the lightest neutrino mass and squared-mass differences. In the normal mass ordering (NO), m_1 is the lightest neutrino; in the inverted ordering (IO), m_3 is the lightest neutrino.

Measurements of neutrino oscillations have also established the parameters of the PMNS matrix, in terms of mixing angles θ_{ij} and a phase angle δ_{CP} related to charge-parity-violation:

$$
U = \begin{bmatrix} 1 & 0 & 0 \\ 0 & \cos\theta_{23} & \sin\theta_{23} \\ 0 & -\sin\theta_{23} & \cos\theta_{23} \end{bmatrix} \begin{bmatrix} \cos\theta_{13} & 0 & \sin\theta_{13}\, e^{-i\delta_{CP}} \\ 0 & 1 & 0 \\ -\sin\theta_{13}\, e^{i\delta_{CP}} & 0 & \cos\theta_{13} \end{bmatrix} \begin{bmatrix} \sin\theta_{12} & \cos\theta_{12} & 0 \\ -\cos\theta_{12} & \sin\theta_{12} & 0 \\ 0 & 0 & 1 \end{bmatrix}.
$$
(2.3.2)

Using the current best-fit values of the parameters $\theta_{12} = 33.44^{\circ+0.78}_{\ \ -0.75}$, $\theta_{13} = 8.57^{\circ+0.13}_{\ \ -0.12}$, $\theta_{23} = 49.0^{\circ+1.1}_{\ \ -1.4}$ and $\delta_{CP} = 195^{\circ+51}_{\ \ -25}$ from [19] [20], the squared absolute values of the PMNS matrix are

$$
|U|^2 \simeq \begin{bmatrix} 0.68 & 0.30 & 0.02 \\ 0.07 & 0.37 & 0.56 \\ 0.25 & 0.34 & 0.42 \end{bmatrix}.
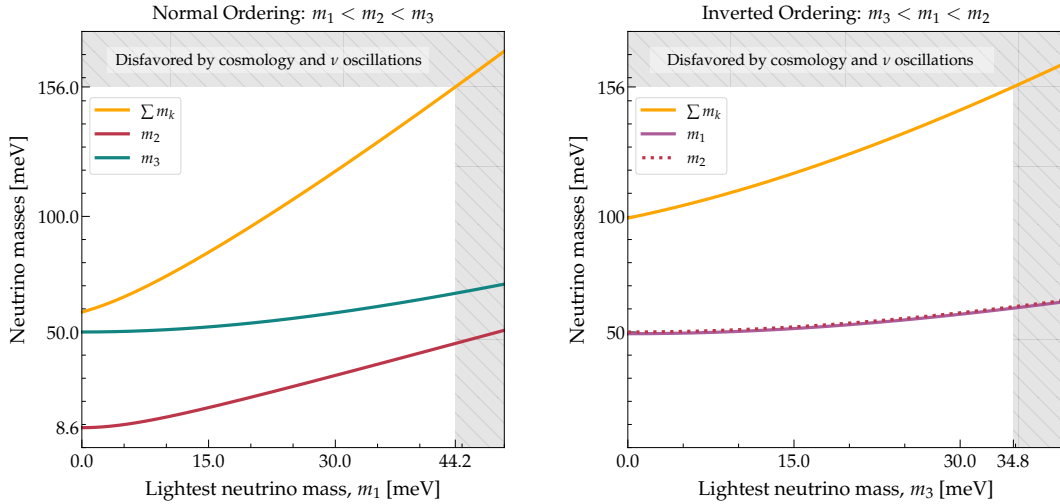$$
(2.3.3)

Figure 2: Current allowed ranges of the neutrino masses in the normal (*left*) and inverted (*right*) mass ordering. The shaded regions are disfavored by the upper limit of $\sum_i m_i < 156$ meV from cosmology, combined with the current best-fit values of the mass-squared differences from Ref. [27].
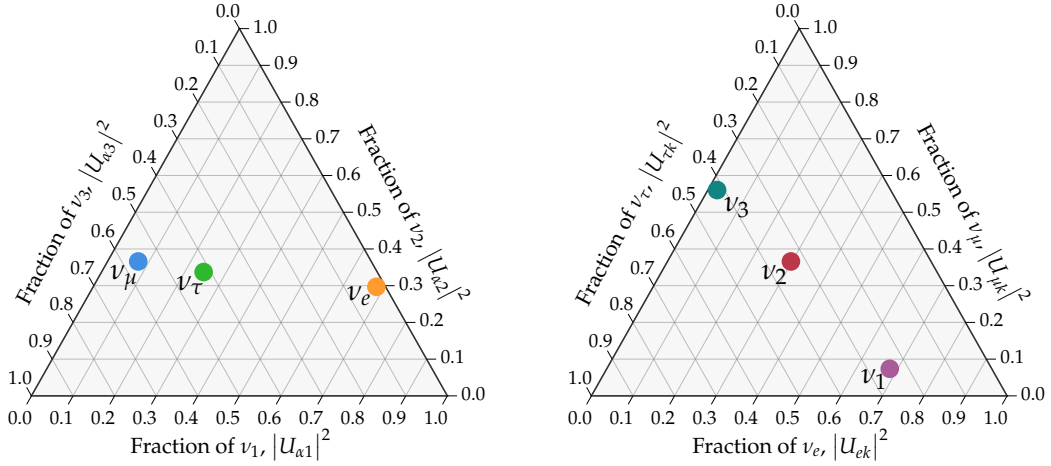
Figure 3: A graphical representation of the PMNS matrix, Eq. (2.3.3). (*Left*) mass-eigenstate content of each neutrino flavor. (*Right*) flavor content of each mass eigenstate. Computed using the current best fit values of the neutrino mixing angles and Dirac mass phases from Ref. [27].

These calculated values can be interpreted as the mass composition ratios of each of the three neutrinos flavors since $\sum_i |U_{\alpha i}|^2 = 1$. Figure 3 shows a graphical representation of both the flavor and mass ratios of neutrinos using the PMNS matrix from Eq. (2.3.3).

The mass eigenstate ν_k propagating in vacuum evolves with time as:

$$|\nu_k(t)\rangle = e^{-iHt} |\nu_k\rangle = e^{-iE_k t} |\nu_k\rangle \ , \qquad (2.3.4)$$

where $E_k = \sqrt{\bar{p}^2 + m_k^2}$ is the total relativistic energy of the neutrino. By means of neutrino mixing equation (2.3.1) we can rewrite equation (2.3.4) as:

$$|\nu_\alpha(t)\rangle = \sum_k U^*_{\alpha k} |\nu_k(t)\rangle = \sum_k U^*_{\alpha k} \, e^{-iE_k t} |\nu_k\rangle \, . \qquad (2.3.5)$$

Since neutrino states are orthogonal ($\langle \nu_j | \nu_k \rangle = \delta_{jk}$) the probability of a neutrino ν_α to be found as ν_β after time t is:

$$P_{\nu_\alpha \to \nu_\beta}(t) = \left| \langle \nu_\beta | \nu_\alpha(t) \rangle \right|^2 = \left| \sum_k U^*_{\alpha k} U_{\beta k} \, e^{-iE_k t} \right|^2 . \qquad (2.3.6)$$

In the limit of ultra-relativistic neutrinos traveling with velocities very close to the speed of light, their energies become $E_k \simeq E + m_k^2/2E$ where E is the neutrino energy excluding mass contributions. In neutrino oscillation experiments it is generally very difficult to have control of and measure the propagation time of the neutrinos t. In

the ultra-relativistic limit becomes where $L \simeq t$ we get the following expression for the transition probability:

$$P_{\nu_\alpha \to \nu_\beta}(L, E) \simeq \sum_{k,j} U^*_{\alpha k} U_{\beta k} U_{\alpha j} U^*_{\beta j} \exp\left(-i\frac{\Delta m^2_{kj} L}{2E}\right), \qquad (2.3.7)$$

where $\Delta m^2_{kj} \equiv (m^2_k - m^2_j)$ is the squared-mass difference. This expression is particularly useful when studying the flavor oscillation of very high energy neutrinos traveling en route to Earth.

2.4 NEUTRINO SECRET INTERACTIONS

We mentioned earlier that neutrinos only interact gravitationally and via the weak force. Within the *Standard Model* (SM), interactions between two neutrinos are particularly weak, making them irrelevant for most physical processes except for a handful of cases involving huge neutrino densities. Currently there are a number of observed physical phenomena which the SM fails to explain. Extending the SM to allow stronger self-interactions between neutrinos known as *secret neutrino interactions* (νSI) introducing a new mediator can help explain the problems mentioned above. To name a few:

1. **Origin of the Neutrino Mass:** Neutrinos can change from one flavor to another. This implies that the neutrino must have a mass. Neutrinos within the SM are however massless and there is no mechanism in the SM that might give mass to the neutrino [28–33].

2. **The Muon Anomalous Moment:** The computed value of the muon magnetic dipole moment in the SM does not match the one measured from experiments. Physicists believe that the reason for this mismatch is some currently unknown physics, that when accounted for will add missing contributions to the computed value [34, 35].

3. **Tension in Cosmology:** Historically the Hubble parameter H_0 (the expansion rate of the universe) has been determined by comparing the receding velocities of nearby galaxies to their distance away by measuring their redshift and luminosity respectively. Using modern space telescopes physicists have applied this method to deduce the value of H_0 to be around 73 km s^{-1} Mpc^{-1} with very high precision. However, recent detailed measurements of irregularities in the CMB result in a value of H_0 closer to 68 km s^{-1} Mpc^{-1}. This is the resulting tension in cosmology, where we now have two different values of H_0 that were determined with high level of certainty in both cases. A plausible solution to resolve this tension is that there might exists some unknown physics, that when accounted for can affect the calculated value of H_0 from CMB measurements [1, 36–38].

4. **The LSND Anomaly:** The Liquid Scintillator Neutrino Detector (LSND) at the Los Alamos National Laboratory was set up to look for evidence of neutrino oscillations. It resulted in a measurement of a fraction of produced neutrinos to anti-neutrinos which can not be described by the three SM neutrinos [39].

Currently there is no evidence pointing towards the existence of νSI, but searches have set the allowed regions for the mediator mass and coupling strengths of these new interactions [16]. However with recent developments in neutrino telescope technology, we are now able to detect neutrinos of increasingly higher energies with greater sensitivity. Neutrinos with energies in the range of TeV–PeV have been detected at the IceCube neutrino observatory, and with upcoming upgrades in IceCube-Gen2 [40] we hope to be able to detect the first UHE neutrinos with energies in the range of PeV–EeV. Measurements of these very high energy neutrinos show that their sources seem to be isotropic, suggesting that they are mostly of extra-galactic origin. Being extra-galactic indicates that these neutrinos have a very long baseline as they propagate on their way to Earth, which makes them a great candidate to test the existence of νSI. While propagating over long distances, neutrinos can interact with relic background neutrinos such as the CνB and create a pair of two new neutrinos, redistributing both neutrino flavors and the initial pair energy. Thus even though νSI are believed to be extremely weak, given a long enough baseline these interactions might leave imprints and features such as dips and pileups on the neutrino energy spectra detected on Earth.

We consider a simple model for νSI via a new scalar mediator ϕ of mass m_ϕ and a corresponding interaction Lagrangian

$$\mathcal{L} = \phi \sum_{ij} g_{ij} \bar{\nu}_i \nu_j, \tag{2.4.1}$$

where g_{ij} are the coupling strengths between two neutrino mass eigenstates $i, j \in \{1, 2, 3\}$. We also define a 3×3 coupling matrix $\mathbf{G}$ for conventional purposes:

$$\mathbf{G} \equiv \begin{pmatrix} g_{11} & g_{12} & g_{13} \\ g_{21} & g_{22} & g_{23} \\ g_{31} & g_{32} & g_{33} \end{pmatrix}. \tag{2.4.2}$$

We are interested in the scenario where an UHE neutrino scatters off a low-energy CνB neutrino.

For $g_{ij} \sim 0.01$ or lower, νSI cross-sections emerging from the Lagrangian (2.4.1) for an incoming UHE neutrino scattering off a CνB neutrino are dominated by s-channel contributions [41]. Figure 4 shows a Feynman diagram for the νSI s-channel process. Thus we take the cross-section to have a Briet-Wigner form

$$\sigma_{ijkl}(E) = \frac{|g_{ij}|^2 |g_{kl}|^2}{4\pi} \frac{s_j}{[s_j - m_\phi^2]^2 + (m_\phi)^2 \Gamma_\phi^2}, \tag{2.4.3}$$

for the scattering process $\nu_i \nu_j \to \nu_k \nu_l$ where $s_j = 2E m_j c^2$ is the center-of-mass energy and Γ_ϕ is the decay width:

$$\Gamma_\phi = \left(\sum_{ij} |g_{ij}|^2 \right) m_\phi / (4\pi). \tag{2.4.4}$$

Here we have taken a relativistic limit for the center-of-mass energy s_j, where the energy E of the incoming UHE neutrino is much greater than the energy of a target CνB neutrino ν_j, that we take to be at rest. Looking at equation (2.4.3) the
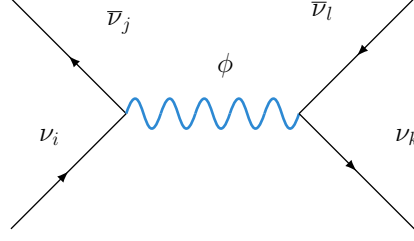
Figure 4: Feynman diagram for the s-channel νSI process emerging from the interaction Lagrangian in equation (2.4.1).

cross-section is maximized when $s_j = (m_\phi c)^2$, thus we expect a peak resonance of νSI at energies E_j of the incoming UHE neutrinos at

$$E_j = \frac{m_\phi^2}{2m_j}. \tag{2.4.5}$$

The scattering cross-section in equation (2.4.3) can be further simplified for practical computational purposes. The full width at half maximum of the resonance is identified by the energy interval where $[s_j - m_\phi^2]^2 < (m_\phi)^2 \Gamma_\phi^2$. Given a detector with energy resolution of ΔE, if the width of the resonance is smaller than the resolution of the detector, one can approximate the scattering cross-section to be a δ-function. Expanding the center-of-mass energy s_j in terms of the resonance energies E_j in the inequality above one finds that the δ-function approximation is valid when $2E_j \Gamma_\phi / (m_\phi) < \Delta E$, and the resulting cross-section is

$$\sigma_{ijkl}(E) = \sigma_R^{ijkl} E \delta(E - E_j), \tag{2.4.6}$$

where $\sigma_R^{ijkl} = (\hbar c)^2 |g_{ij}|^2 |g_{kl}|^2 / [4(m_\phi c^2)\Gamma_\phi]$. The interaction rate of an UHE energy neutrino ν_i propagating through the CνB can thus be expressed as

$$\Gamma_i \equiv \sum_j n_j(z) \sigma_R^{ij} c, \quad \sigma_R^{ij} \equiv \sum_{kl} \sigma_R^{ijkl}, \tag{2.4.7}$$

summing over all possible scattering cross-sections of possible mass eigenstates of both target CνB neutrinos and the produced neutrino pairs, where $n_i(z) = 56(1 + z)^3$ cm^{-3} [42] is the number density of CνB neutrinos.

The existence of νSI has previously been tested for high-energy astrophysical neutrinos in the TeV-PeV range using 6 years of accumulated data from IceCube [16]. Reference [16] found no significant evidence for the existence of νSI, but placed competitive limits on both the coupling strengths and mediator mass of νSI, shown in the region marked as "IceCube HESE 6 years (this work)" in Fig. 5 taken from the same reference. There we can see additional contributions from different sources to the νSI coupling strengths and mediator mass limits mentioned in chapter 1. The detection of UHE neutrinos will allow us to probe mediator masses in the > 100 MeV range, where bounds are currently weak. We are thus interested in expanding the search for νSI to UHE neutrinos with focus on cosmogenic neutrinos.
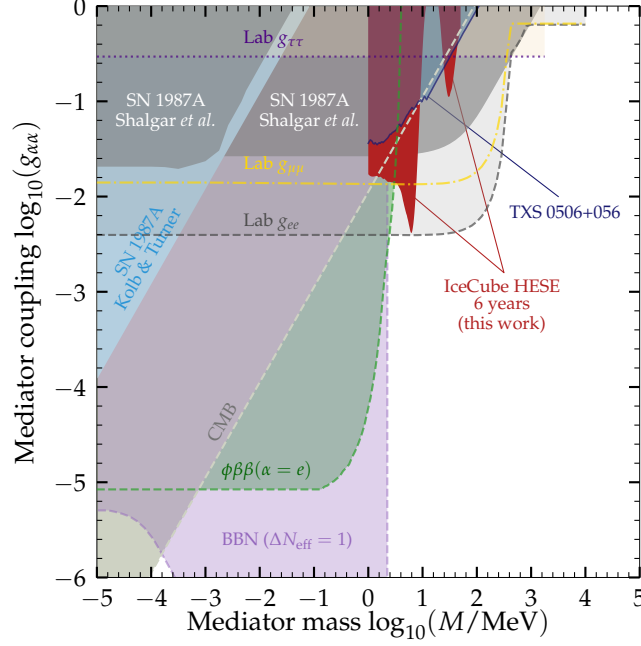
Figure 5: Limits on the mass m_ϕ and coupling strengths $g_{\alpha\alpha}$ ($\alpha = e, \mu, \tau$) of the new mediator of νSI. Unless otherwise stated, each limit applies to all flavors, i.e., $g_{ee} = g_{\mu\mu} = g_{\tau\tau}$. Shaded regions are disfavored. Original figure taken from [16].

2.5 COSMOGENIC NEUTRINOS

Cosmogenic neutrinos are produced when *ultra-high-energy cosmic rays* (UHECRs) propagate through intergalactic medium and interact with cosmic photons such as the CMB and the cosmic infrared background. The UHECR protons and nuclei interact with background photons via e^+e^- pair production or photo-hadronic interactions, producing neutrinos and other side products. When UHECR protons reach energies of around 5×10^{19} eV they can trigger pion production by interacting with CMB photons, producing either a neutral pion π^0 or positively charged pion π^+, where π^+ decays into muon μ^+ and a muon neutrino ν_μ. The π^+ can then further decay into an electron neutrino ν_e and a muon anti-neutrino $\bar{\nu}_\mu$ [43]. In these kind of cascades around 1/20th of the initial proton energies get converted into neutrinos. The full decay process for the production of cosmogenic neutrinos is thus:

$$p + \gamma_{\text{CMB}} \rightarrow \Delta \rightarrow \begin{cases} p + \pi^0 \rightarrow p + \gamma + \gamma \\ n + \pi^+ \rightarrow n + \mu^+ + \nu_\mu \rightarrow n + e^+ + \nu_e + \bar{\nu}_\mu + \nu_\mu \end{cases} . \quad (2.5.1)$$

Cosmogenic neutrinos are thus produced with flavor ratios $(f_{\nu_e} : f_{\nu_\mu} : f_{\nu_\tau}) = (1/3 : 2/3 : 0)$ where f_{ν_α} is fraction of produced neutrinos of flavor α. Here we added the combined contribution of neutrino and anti-neutrinos for the flavor ratios, since high-energy neutrino telescopes like IceCube find it challenging to distinguish between the two.

Looking at ultra-relativistic neutrino-oscillation flavor transition-probabilities from equation (2.3.7), we can separate it in terms of stationary and oscillatory components as

$$P_{\nu_\alpha \to \nu_\beta}(L, E) = \sum_k |U_{\alpha k}|^2 |U_{\beta k}|^2 + 2\,\mathrm{Re} \sum_{k>j} U_{\alpha k}^* U_{\beta k} U_{\alpha j} U_{\beta j}^* \exp\left(-2\pi i \frac{L}{L_{kj}^{\mathrm{osc}}} \right) , \quad (2.5.2)$$

where $L_{kj}^{\mathrm{osc}} \equiv 4\pi E / \Delta m_{kj}^2$ is the oscillation length. In the case of cosmogenic neutrinos with energies $E \sim$ EeV and baselines $L \sim$ Gpc the oscillation length becomes roughly of the order of $L_{kj}^{\mathrm{osc}} \sim 0.1$ pc calculated using the current best-fit values of the mass differences [27]. Thus we can expect cosmogenic neutrinos to have undergone around $\sim 10^{10}$ oscillation cycles before they would arrive on Earth, making it impossible to resolve neutrino oscillations in any meaningful way. Instead we can make use of the average flavor-transition probabilities of cosmogenic neutrinos detected on Earth as:

$$\left\langle P_{\nu_\alpha \to \nu_\beta} \right\rangle = \sum_k |U_{\alpha k}|^2 |U_{\beta k}|^2 . \quad (2.5.3)$$

Consequently we can expect the specific flavor fractions of cosmogenic neutrinos on Earth to be:

$$f_{\nu_\alpha, \oplus} = \sum_\beta \left\langle P_{\nu_\beta \to \nu_\alpha} \right\rangle f_{\nu_\beta, S} . \quad (2.5.4)$$

There is no longer any dependence on the neutrino mass differences, thus the average transition probability is solely determined by the phase and mixing angles from the PMNS matrix. Even though no ν_τ are not produced during charged pion decays, given a long enough baseline they can emerge from flavor oscillations of other cosmogenic neutrinos during propagation. Figure 6 shows an example of such flavor ratio evolutions for a few relevant initial configurations.
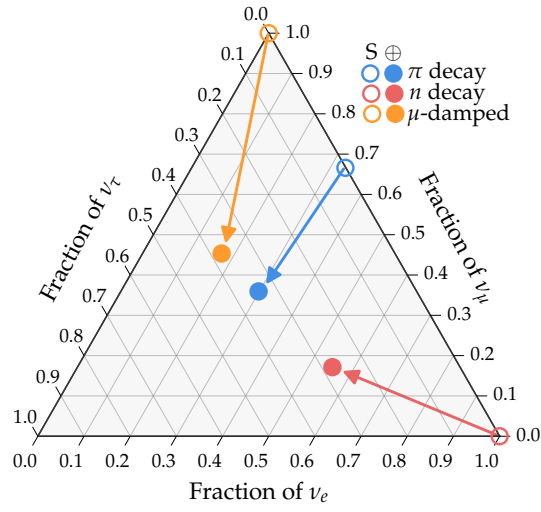
Figure 6: Ternary plot showing the evolution of neutrinos flavor ratios using an averaged flavor transition probability calculated using neutrino mixing angles obtained from νfit [27]. We showcase three benchmark scenarios of flavor ratios at the sources: full pion-decay ("π decay"), pion decay where the intermediate muon cools via synchrotron radiation before decaying ("μ-damped"), and $\bar{\nu}_e$ production via beta decay of neutrons ("n decay"). S marks the flavor composition at source and $\oplus$ marks the average flavor ratio probability after neutrino oscillations. Ternary plot generated using [44].

NEUTRINO PROPAGATION

3.1 HIGH-ENERGY NEUTRINO PROPAGATION

We are interested in exploring the effects of νSI on a flux of neutrinos propagating through the CνB. Given a long enough baseline, relatively weak self-interactions can have significant effects on the UHE neutrino spectrum, redistributing the neutrino energies, leaving possible dips and pileups in the spectrum.

We follow the formalism from Ref. [45] to write the propagation equation. We choose to work in the neutrino mass basis where νSI take place, and later convert our results to the flavor basis. In comoving coordinates we define the flux $\Phi_i(t, E)$ to be the number density of high-energy neutrinos ν_i per unit conformal time per unit comoving area per unit energy. The dynamics of Φ_i are described by a Boltzmann equation written in the neutrino mass basis:

$$\frac{\partial \Phi_i}{\partial t} = H\Phi_i + HE\frac{\partial \Phi_i}{\partial E} + S_i(t, E) - \Gamma_i(t, E)\Phi_i + S_{\text{re-inj},i}(t, E). \qquad (3.1.1)$$

Here, $H(z) = H_0\left[\Omega_m(1+z)^3 + \Omega_\Lambda\right]^{1/2}$ is the Hubble factor (expressed in redshift z instead of time t where $H_0 = 67.4$ km s^{-1} Mpc^{-1} is the Hubble constant) dictating the expansion rate of the universe ($\Omega_m = 0.315$ and $\Omega_\Lambda = 0.685$ are the contemporary values of the energy density fractions of matter and dark energy respectively) with parameter values taken from the Particle Data Group [46]. The production rate of neutrinos S_i accounts for injected contributions to the neutrino flux from external sources. The absorption rate of neutrinos due to νSI with the CνB is denoted by Γ_i, and $S_{\text{re-inj},i}$ is the re-injection rate of ν_i from scattering of the flux $\Phi_j(t, E')$ with the CνB neutrinos of densities $n_k(t)$ via νSI as

$$S_{\text{re-inj},i}(t, E) = \sum_{jkl} n_k(t)c \int_E^\infty dE' \Phi_j(t, E') \left[\frac{d\sigma_{jkil}(E', E)}{dE} + \delta_{il}\frac{d\sigma_{jkil}(E', E' - E)}{dE}\right], \quad (3.1.2)$$

accounting for all possible incoming neutrino energies E' and summed over all possible scattering cross-sections $\sigma_{jkil}(E', E)$, including a Kronecker δ-term accounting for the possibility of upscattering to two neutrinos of the same mass eigenstate.

A difficulty arises when trying to solve equation (3.1.1) analytically since the re-injection term $S_{\text{re-inj},i}$ contains an integral of the neutrino flux itself, that results in a non-closed form solution. To get around this obstacle we apply a δ-function approximation for the scattering cross-section σ_{jkil} according to equation (2.4.6).

Converting from time t to redshift z via the relation $dz/dt = -H(z)(1+z)$ and integrating up to $z_{\max}$, we can solve (3.1.1) analytically as

$$\Phi_i(z, E; m_\phi, \mathbf{G}, \mathbf{m}_\nu) = \frac{1}{1+z} \int_z^{z_{\max}} \frac{dz'}{H(z')} e^{-\tau_i(z',z,E)} \tilde{S}_i\left[z', \left(\frac{1+z'}{1+z}\right)E\right], \quad (3.1.3)$$

$$\tilde{S}_i(z, E; m_\phi, \mathbf{G}) = S_i(z, E) + S_{\text{re-inj},i}(z, E), \quad (3.1.4)$$

$$S_{\text{re-inj},i}(z, E) = \sum_{jkl}(1 + \delta_{il})\Gamma_R^{jkil}\Phi_R^{jk}(z, E)\Theta(E_k - E). \quad (3.1.5)$$

The solution can roughly be understood as follows: We add contributions to the high-energy neutrino flux by integrating from z to $z_{\max}$ the total injection rate $\tilde{S}_i$, accounting for redshifting of the injected neutrino energies over time. The optical depth of a neutrino ν_i of energy E, propagating over a time interval from z to z' is denoted by $\tau_i(z', z, E)$. The Φ_R^{jk} term denotes the neutrino flux Φ_j evaluated close to one of the resonant energies E_k according to equation (2.4.5). A more detailed explanation of the included terms and derivations can be found in Appendix A. The computed neutrino fluxes can then be converted to the neutrino flavor basis by the use of the PMNS matrix U as

$$\Phi_\alpha(t, E) = \sum_i |U_{\alpha i}|^2 \Phi_i(t, E). \quad (3.1.6)$$

3.2 INJECTING COSMOGENIC NEUTRINOS

To solve equation (3.1.3) we need the neutrino injection rate term S_i.

To evaluate the injection rate of cosmogenic neutrinos we make use of the *Propagation including Nuclear Cascade equations* code PRINCE [47], following the work from Ref. [43]. PRINCE is an UHECR propagation equation solver that uses a generic model of the production of UHECR, evolves the contributions with redshift and normalizes the flux of UHECRs by fitting it to UHECR spectrum and mass-composition data from the Pierre Auger Observatory [48, 49]. PRINCE computes the flux of cosmogenic neutrinos propagated from a chosen initial redshift down to a final redshift decremental steps. At each redshift step it adds contributions to the neutrino flux from photohadronic interactions of the UHECRs on the CMB and the extragalactic background light, accounting for the photodisintegration of UHECR nuclei during propagation, redshifts the energy of the flux and accounts for changes in the flavor ratios due to neutrino oscillations.

Unlike neutrinos that can traverse through the cosmos practically undisturbed, UHECRs are prone to interacting, leading to energy losses while propagating through the intergalactic medium. This leads to UHECRs having an effective horizon, limiting the distance that they can propagate until they have lost sufficient amount of energy. For UHE cosmic protons the effective horizon is ~ 75 Mpc [50]. PRINCE approximates all known continuous source density functions within the UHECR horizon $z \lesssim 1$ following the star formation rate as shown in equation (3.2.1), where $m = 4.2$ is the best fit value with to data from the Pierre Auger Observatory [43]. For
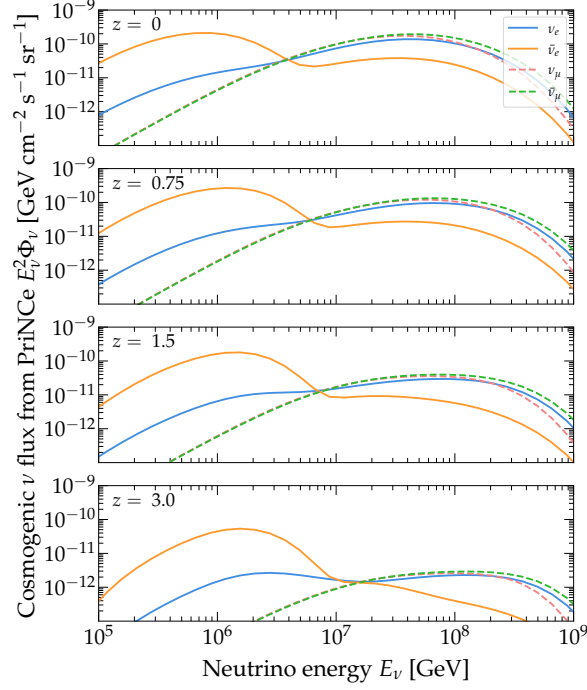
Figure 7: Fluxes of cosmogenic neutrinos generated by PRINCE from an initial redshift of $z = 4$ and varying final redshifts. The fluxes are parameterized and normalized by fitting generated UHECR fluxes at a redshift of $z = 0$ and their mass composition with UHECR data from the Pierre Auger Observatory.

the generation of UHECRs beyond $z = 1$ that participate in producing secondary messengers such as neutrinos, little is know about their source densities. To account for this PRINCE makes the following approximation of freezing out the source density evolution for redshifts $z \geq 1$ as

$$n_{\text{evol}}(z) = \begin{cases} (1+z)^m \,, & z \leq 1 \\ (1+z)^m \big|_{z=1} \,, & z \geq 1 \end{cases} .$$ (3.2.1)

Figure 7 showcases a cosmogenic neutrino flux from PRINCE computed at different redshifts. There we see a gradual buildup of the fluxes while propagating down to a redshift of $z = 0$. There is a clear deficit in flux of $\bar{\nu}_e$ at high energies compared to the other neutrino flavors since they are not produced during charged pion decays. At lower energies we see that the neutrino flux is dominated by $\bar{\nu}_e$ produced during beta decays of UHECRs.

To solve equation (3.1.3), we need the injection rate of cosmogenic neutrinos. We numerically compute the injection rate of cosmogenic neutrinos of each flavor $S_{\nu_\alpha}(z, E)$ by comparing the cosmogenic neutrino fluxes $\Phi_{\nu_\alpha}(z, E)$ from PRINCE of neighbouring energies and redshifts as

$$S_{\nu_\alpha}(z, E) \simeq \frac{(1+z)H(z)}{\Delta z} \left\{ \Phi_{\nu_\alpha}(z, E) - \left(\frac{1+z+\Delta z}{1+z} \right) \Phi_{\nu_\alpha} \left[z + \Delta z, \left(\frac{1+z+\Delta z}{1+z} \right) E \right] \right\},$$
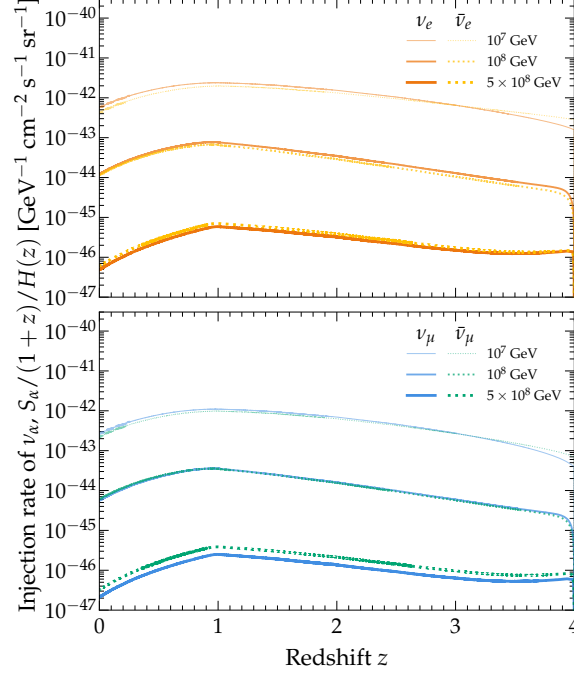(3.2.2)

17

Figure 8: Injection rate of cosmogenic neutrinos computed with PRINCE as a function of redshift z shown at constant energies.

where Δz is the chosen propagation redshift step size from (in our case $\Delta z = 10^{-3}$). The computed injection rate S_α can then be converted to the neutrino mass basis using the PMNS U as

$$S_i(t, E) = \sum_\alpha |U_{\alpha i}|^2 S_\alpha(t, E). \qquad (3.2.3)$$

Figure 8 illustrates the computed injection rate of cosmogenic neutrinos from PRINCE using the same data used for generating the cosmogenic neutrino fluxes shown in Fig. 7. There is a sharp peak in the injection rate at the UHECR horizon $z = 1$. Since ν_τ are not produced in charged pion decay they do not contribute to the injection of cosmogenic neutrinos, but they appear via oscillations.

3.3 NEUTRINO FLUX AT EARTH

We solved equation (3.1.3) to predict the flux of cosmogenic neutrinos at Earth ($z = 0$) under the effects νSI using an injection rate computed with PRINCE, propagating cosmogenic neutrinos down from a redshift $z_{\max}$:

$$\Phi_i(0, E; m_\phi, \mathbf{G}, \mathbf{m}_\nu) = \int_0^{z_{\max}} \frac{dz'}{H(z')} e^{-\tau_i(z', 0, E)} \tilde{S}_i \left[z', \left(1 + z' \right) E \right]. \qquad (3.3.1)$$

As discussed in chapter 3.2, little is known about the source evolution of UHECRs that contribute to the production of cosmogenic neutrinos past a redshift of $z \sim 1$. Thus it is sensible to consider two different cases for the choice of $z_{\max}$: a conservative
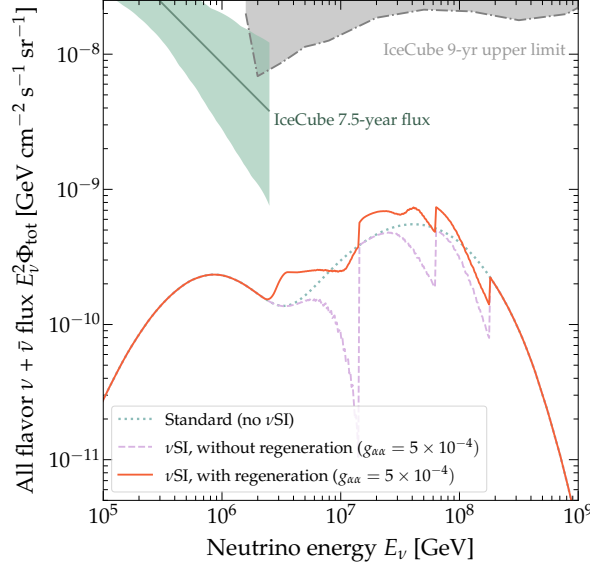
Figure 9: Flux of cosmogenic neutrinos at Earth summed over over all flavors, propagated down from a redshift of $z = 4$. Generated with the following set of parameters specifically chosen to illustrate the effects of νSI: $m_\phi = 10^{7.7}$ eV, $\mathbf{m}_\nu = [0.088, 0.02, 0.007]$ eV and $g_{\alpha\alpha} = 5 \times 10^{-4}$ where we take the νSI coupling matrix to be flavor-universal and diagonal. To better showcase the effects of νSI we include three different lines on the plot, one for the neutrino flux without the presence of νSI, another for νSI with depletion but no regeneration (meaning that we only account for depletion of neutrinos during νSI scattering but exclude all possible re-injection of neutrinos). A flux of detected high-energy neutrinos from 7.5 years of IceCube data [51] and an upper limit on the flux of UHE neutrinos from 9 years if IceCube data [52] are shown as shaded regions.

case where sources contribute only up to $z_{\max} = 1$, as in Ref. [43], and a more realistic case with $z_{\max} = 4$. We chose to explore the realistic case of $z_{\max} = 4$.

Figure 9 shows a sample resulting cosmogenic neutrino flux at Earth from PRINCE with and without the presence of νSI. As shown in equation (2.4.5) we expect a depletion of neutrinos at and right below the energies E_j where the scattering of cosmogenic neutrinos with the CνB becomes resonant. Post scattering two neutrinos are re-injected into the neutrino flux at lower energies below the resonances. This in combination with redshifting of the neutrino energies during propagation leads to characteristic dips and pileups on the cosmogenic neutrino flux at Earth around the resonance energies E_j. The sensitivity regions of the detection rate of neutrinos of such energies are also shown graphically on the figure based on the currently available data from IceCube.

Figure 10 shows the flavor ratios of cosmogenic neutrinos at Earth for an illustrative set of free parameters m_ν, m_ϕ and $g_{\alpha\beta}$ as a function of energy. Below ~ 5 PeV the fluxes are dominated by $\bar{\nu}$ from the decay of neutrons into $\bar{\nu}_e$, and the oscillation of $\bar{\nu}_e$ into $\bar{\nu}_\mu$ and $\bar{\nu}_\tau$. Above ~ 5 PeV the fluxes are dominated by ν_μ and $\bar{\nu}_\mu$ from photopion production. The bottom panel shows effects of νSI right below the first energy resonance E_1 where neutrinos redshifted down to lower energies by a factor of $(1+z)|_{z=4}$ as described by the last term under the integral in equation (3.3.1) have more leveled out flavor ratios compared to the case of no νSI.
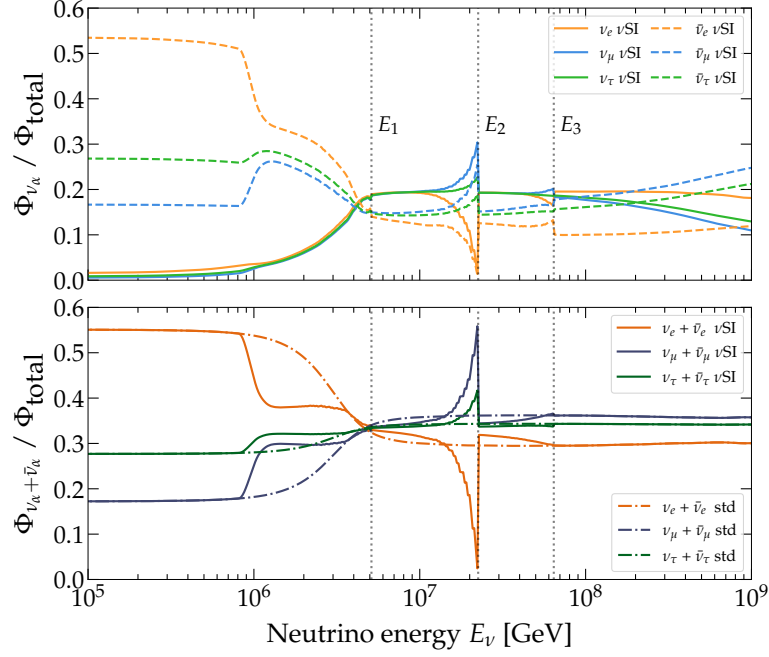
Figure 10: Flavor ratios of cosmogenic neutrino fluxes at Earth as a function of energy. The top graph shows the flavor ratios of all flavors including their antiparticle counterparts. The bottom panel shows the combined flavor ratios of neutrinos and ant-neutrinos plotted against flavor ratios of the same computed neutrino flux without the presence of νSI. Generated assuming: $z_{\max} = 4$, neutrino masses of $\mathbf{m}_\nu = [0.088, 0.02, 0.007]$ eV, a mediator mass of 50 MeV and $g_{\alpha\alpha} = 5 \times 10^{-4}$ where the νSI coupling matrix was taken to be flavor-universal and diagonal. The resonant energies E_j are indicated with black dotted lines.

We now turn our attention to how the neutrino flux at Earth responds to individual changes in our model parameters. The mediator mass m_ϕ shows up in a handful of terms in our propagation equation that have a major effect on the look and shape of the cosmogenic neutrino flux. From equation (2.4.5) we see that $E_j \sim m_\phi^2$, thus lowering or raising the mediator mass m_ϕ will shift the resonances E_j to lower and higher energies, consequently moving the positions of the resonance dips and pileups of our cosmogenic neutrino flux. The mediator mass also appears in the scattering cross-section of νSI as $\sigma_R^{ijkl} \sim m_\phi^{-2}$ as seen from equations (2.4.6) and (2.4.4). Thus for larger m_ϕ we can expect the effects of νSI to become significantly weaker, reducing the height and spread of the pileups of our cosmogenic neutrinos flux at Earth as the likelihood of scattering with the CνB gets smaller.

Figure 11 shows a computed flux of cosmogenic ν_μ at Earth with varying mediator mass m_ϕ keeping all other model parameters fixed. With an increase in m_ϕ we see a shift in the location of the resonances to higher energies in addition to a reduction in the amplitude of the pileups and dips right below them.

The νSI couplings $g_{\alpha\beta}$ dictate the strength of νSI between neutrinos of different flavors. The coupling matrix $\mathbf{G}$ can be configured in multiple different ways and might induce stronger interactions for specific neutrino flavors over others. Thus we explore three different scenarios for the configuration of $\mathbf{G}$ and observe how it affects the form and shape of the cosmogenic neutrino flux at Earth, namely:
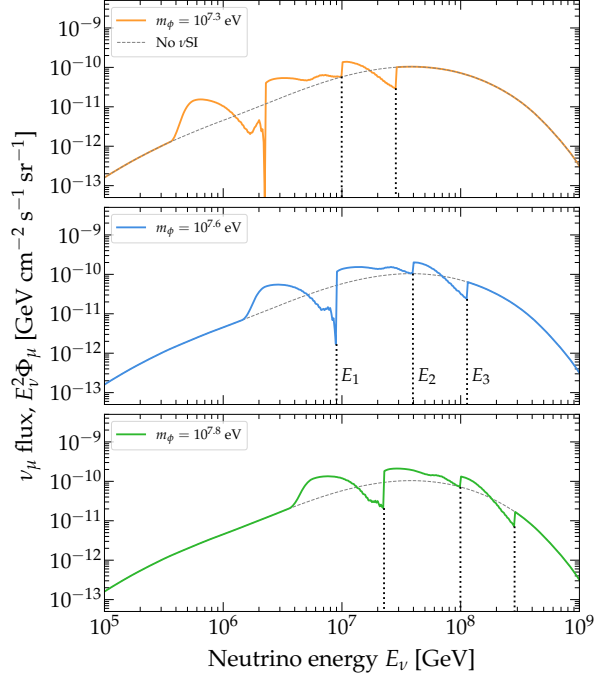
Figure 11: Computed fluxes at Earth of cosmogenic ν_μ neutrinos with varying mediator masses m_ϕ. Generated assuming: $z_{\max} = 4$, neutrino masses of $\mathbf{m}_\nu = [0.088, 0.02, 0.007]$ eV and $g_{\alpha\alpha} = 5 \times 10^{-4}$ where we take the νSI coupling matrix to be flavor-universal and diagonal. The resonance energies E_j are indicated with black dotted lines.

1. **Flavor-diagonal, flavor-universal νSI:** $g_{ee} = g_{\mu\mu} = g_{\tau\tau} = g$; all other couplings fixed to zero

2. **Flavor-diagonal, flavor-non-universal νSI:** g_{ee}, $g_{\mu\mu}$, $g_{\tau\tau}$ independent of each other and freely varying; all other couplings fixed to zero

3. **Tau-only νSI:** $g_{e\tau}$, $g_{\mu\tau}$, $g_{\tau\tau}$ independent of each other and freely varying; all other couplings fixed to zero

In scenarios 1 and 2, two neutrinos of the same flavor can interact with a universal coupling strength g. From our νSI equations (2.4.4) and (2.4.6) we see that the scattering cross-section around the resonances grows with the νSI coupling strength as $\sigma_R^{ijkl} \sim g^2$. Thus for increased coupling strengths we can expect stronger interactions, resulting in larger dips and pileups of neutrinos below the resonances.

Figure 12 shows a sample flux of cosmogenic ν_μ under scenario 1. We can see a noticeable increase in the pileups and dips from down scattered neutrinos under νSI while the locations of the dips are unchanged, as expected from equation (2.4.5) since the resonance energies E_j are not sensitive to changes in the couplings $g_{\alpha\beta}$.

In scenario 3 we wanted to explore the effects of νSI by varying the coupling strengths for ν_τ. For the other flavors, the νSI couplings are zero. Regardless, when changing to the mass basis, the non-zero ν_τ couplings turn on νSI between all mass eigenstates. Still, when converting back to the flavor basis, the effects on the cosmogenic neutrino flux will be more intense for the ν_τ flux than for the ν_e and ν_μ fluxes.

Figure 13 shows an example of a neutrino fluxes under scenario 3 versus scenario 1. Transforming the couplings to the mass basis we find for scenario 1 that $g_{23} \simeq 6.4 \times 10^{-5}$ is especially weak compared to scenario 3 where $g_{23} \simeq 6.3 \times 10^{-3}$. Both ν_μ and ν_τ are heavily populated by ν_3 compared to ν_e that is dominantly populated by ν_1 as can be seen from the ternary plot in figure 3. Thus we can see that the effect of νSI are heavily damped around the resonances E_2 and E_3 for ν_μ and ν_τ in scenario 1 compared to scenario 3.

Below, we use the cosmogenic neutrino fluxes with νSI to compute the expected rate of events for radio component of the upcoming IceCube-Gen2 neutrino telescope. In the cosmogenic neutrino fluxes shown above, the νSI parameters were often strategically chosen for illustrative purposes. From this point onward we follow a more realistic approach by constrain ourselves to normal mass ordering by exploring changes in m_1 instead of $\mathbf{m}_\nu$ as shown in Table 1.
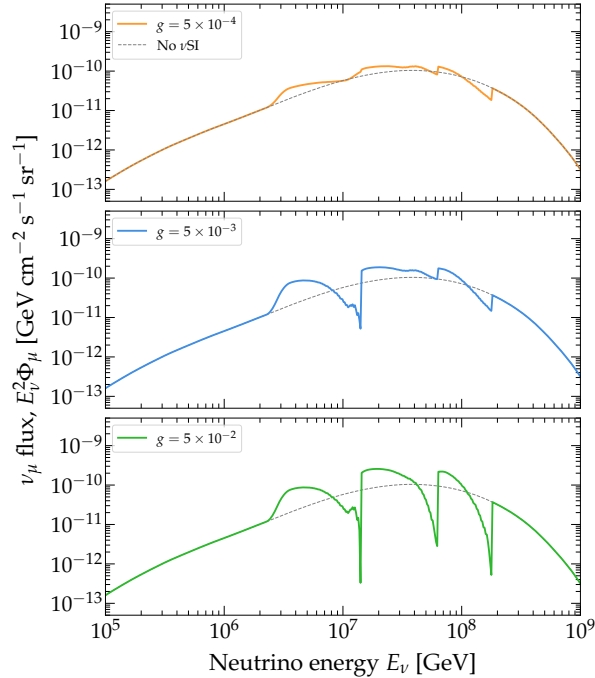
Figure 12: Computed fluxes at Earth of cosmogenic ν_μ neutrinos where we take the νSI coupling matrix to be flavor-universal and diagonal and vary the coupling g. Generated with injected neutrino contributions propagated down from a redshift of $z_{\max} = 4$, a mediator mass $m_\phi = 10^{7.7}$ eV and neutrino masses of $\mathbf{m}_\nu = [0.088, 0.02, 0.007]$ eV.

Figure 13: Comparison of fluxes of cosmogenic neutrinos at Earth for two different coupling scenarios assuming a universal coupling strength. **Scenario 1**: $g_{ee} = g_{\mu\mu} = g_{\tau\tau} = 10^{-2}$. **Scenario 3**: $g_{e\tau} = g_{\mu\tau} = g_{\tau\tau} = 10^{-2}$. Generated with injected neutrino contributions propagated down from a redshift of $z_{\max} = 4$, a mediator mass $m_\phi = 10^{7.7}$ eV and neutrino masses of $\mathbf{m}_\nu = [0.088, 0.02, 0.007]$ eV.

NEUTRINO DETECTION

4.1 ICECUBE

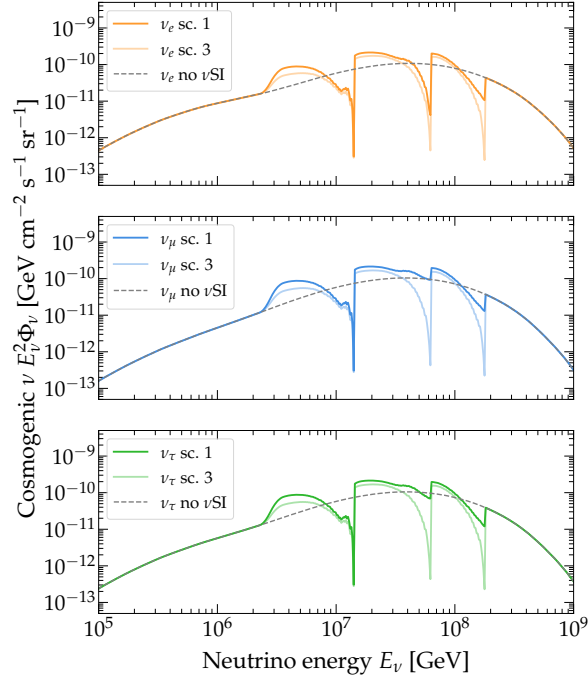The ongoing experiment most capable of observing UHE neutrinos is the IceCube neutrino observatory located at the South Pole. IceCube is a Cherenkov light based detector consisting of over 5000 underground photomultipliers instrumenting about 1 km^3 volume of pure ice.

When a neutrino travels through the Antarctic ice it can interact with a nucleon in the ice via deep inelastic scattering through either neutral-current (NC) neutrino-nucleon interaction, or produce charged leptons via a charged-current (CC) neutrino-nucleon interaction. Both types of interactions can be shown schematically as

$$(\text{NC}) \qquad \nu_\alpha/\bar{\nu}_\alpha + N \rightarrow \nu_\alpha/\bar{\nu}_\alpha + X \,, \qquad (4.1.1)$$

$$(\text{CC}) \qquad \nu_\alpha/\bar{\nu}_\alpha + N \rightarrow l_\alpha^\pm + X \,, \qquad (4.1.2)$$

where N represents a nucleon and X represents the final-state hadrons produced after the break-up of the nucleon. The final-state hadrons and charged leptons initiate particle showers in the ice. When a charged particle in the shower traverses through a dielectric (such as ice) with a speed greater than the phase velocity of light in the medium, it will induce radiation of visible light within the medium. This is known as Cherenkov radiation.

IceCube captures the Cherenkov as it propagates through the ice. The ice is remarkably pure and uniform with an absorption length exceeding 200 m for visible light with wavelengths $\sim$ 400 nm [40]. This makes it possible to sparsely instrument the ice with photomultipliers. Being built deep into the ground, IceCube is shielded from most incoming charged cosmic rays that could contaminate the neutrino signals. It is also shielded from atmospheric muons that arrive to the detector from below. The muons that arrive from above are cleaned using veto techniques, though there is an irreducible background left over that must be accounted for in the analyses. The detected Cherenkov light is then analyzed to deduce information about the incoming neutrinos such as flavor, energy, and incoming angle [53–55].

IceCube has so far detected TeV–PeV neutrinos of astrophysical origin as seen in Figure III.4 of Ref. [51] and in Fig. 9. Despite the success of IceCube it has not discovered UHE neutrinos with energies in the EeV range, because present-day IceCube may be too small to detect the tiny flux of UHE neutrinos. To address the limitation, the planned upgrade IceCube-Gen2 [40], envisioned for the 2030s, is designed to have an effective volume $5 - 7$ times that of IceCube.

Figure 14 shows the outlines of the IceCube-Gen2 upgrades relative to the current configuration of the detector. The addition of new photomultiplier strings
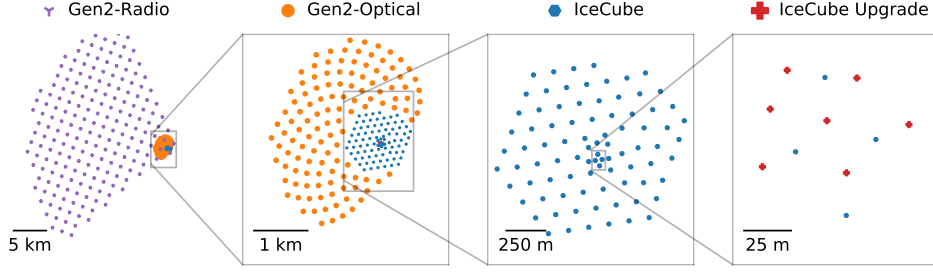
Figure 14: A Schematic figure showing the pending Gen2 upgrades to IceCube compared to the current configuration. The leftmost panel shows the upcoming installation of an array of radio telescopes. The panel second from the left shows the additional strings of photomultipliers that will be installed. The panel second from the right show the current setup at IceCube. The rightmost panel present the upcoming installation of a few additional strings of photomultipliers to increase the detector resolution in a small region. Original figure taken from Ref. [40].

will increase the event statistics, especially towards the higher-energy end of the PeV–TeV neutrino spectrum. In addition, IceCube-Gen2 will contain a radio-detection component consisting in an array of radio antennas buried closer to the surface. The antennas will specifically target UHE neutrinos by looking for the Askaryan emission [56] that they are expected to emit. Below, when computing event rates at the IceCube-Gen2 induced by UHE neutrinos, we do so for its radio-detection component.

Askaryan radiation is produced similarly to Cherenkov radiation, when a neutrino interacts with a nucleon in ice creating a shower of charged secondary particles. The shower particles can ionize nearby ice molecules and positrons in the shower can quickly annihilate with nearby electrons. This creates an evolving charge imbalance between the front and rear of the shower as it propagates. Thus the relativistic particle shower behaves effectively as an accelerating electric dipole producing a coherent emission of radio waves. For in-ice particle showers of energies above EeV, the shower is elongated due to the Landau–Pomeranchuk–Migdal effect, resulting in a greater charge anisotropy producing a more powerful Askaryan radiation [57].

4.2 UHE NEUTRINO PROPAGATION THROUGH THE EARTH

Since neutrinos are weakly interacting, at low energies they are able to reach IceCube from all possible incoming angles. However, because the neutrino-nucleon cross section grows with energy [58–62], at EeV-scale energies the flux of neutrinos is severely attenuated as it propagates through the Earth. We account for this attenuation when predicting event rates in IceCube-Gen2. We characterize the direction of incoming neutrinos by the zenith angle θ_z a neutrino makes with Earth's rotation axis reaching out from the South Pole.

Figure 15 shows schematically how both cosmic and atmospheric neutrinos arrive at Earth and make it to IceCube and their incoming angle θ_z. Neutrinos that arrive from above the South Pole's horizon ($\cos\theta_z > 0$) are recognized as down-going

Figure 15: Illustration of IceCube located at the South Pole and neutrino detection relative to the incoming direction of cosmic particles and the geometry of Earth. The zenith angle an incoming particle makes with the Earth's rotation axis reaching out from the South Pole is marked as θ_z. The yellow dashed arrows show the trajectories of neutrinos. The purple arrows show the trajectories of incoming cosmic rays. The gray arrows show the trajectories of charged leptons. The red stars represent neutrino interactions. Dimensions not to scale. Inspired by Fig. 3 in the paper from Ref. [53].

neutrinos, while neutrinos arriving at IceCube from underneath ($\cos\theta_z < 0$) are called down-going neutrinos.

Just as neutrinos can interact with nucleons in the Antarctic ice inside IceCube, they can interact with nucleons inside the Earth en route to IceCube. Depending on the incoming angle θ_z, neutrinos will travel different distances through the Earth before reaching the detector. NC interactions dampen the energy of the propagating neutrinos, while CC interactions remove neutrinos from the flux. The internal density of Earth has to be taken into account when computing the propagation of neutrinos through the Earth, since denser regions induce more interactions. We do this by adopting the Preliminary Reference Earth Model [63], which models the density radially from the center of the Earth, as a series of concentric layers.

Some of the in-Earth neutrino interactions can produce flavor-specific effects in the neutrino flux that reaches the detector, such as the Glashow resonance and ν_τ regeneration. The Glashow resonance refers to a threshold energy of about $E \simeq 6.3$ PeV when the process $\bar{\nu} + e^- \to W^-$ becomes resonant, reducing the flux of $\bar{\nu}_e$ reaching IceCube while propagating through Earth. A CC-interaction of an UHE ν_τ with an in-Earth nucleon generates a high-energy τ that propagates over a macroscopic distance, losing some energy along the way before quickly decaying back to a ν_τ. This leaves the flux of UHE ν_τ much less attenuated compared to other neutrino flavors as an effect known as ν_τ-regeneration.

To account for these attenuation effects on a flux of cosmogenic neutrinos, when we compute the expected event rates at IceCube-Gen2 (see equation (4.3.3)), we add the contributions from all incoming angles θ_z for each neutrino energy, taking into account propagation properties, traversed distance through the Earth, and possible interactions along the way that can result in attenuation of the final flux at the detector. This was done using NuPropEarth [58] [1], which uses the state-of-the-art computations of the neutrino-matter cross sections including the leading-process deep inelastic scattering of neutrinos on nucleons, and the contributions from sub-leading interactions like scattering off the photon field of nucleons and nuclei, and the scattering on atomic electrons via the Glashow resonance.

Figure 16 shows the transmission probability of UHE neutrinos of different flavors as they traverse through the Earth on their way to IceCube. The attenuation is similar for ν_e and ν_μ where the transition probability falls off with increased neutrino energy E_ν and a steeper incoming angle θ_z. There is much less attenuation for ν_τ compared to the other flavors due to ν_τ regeneration.

Figure 17 shows histograms of the spectrum of UHE energy neutrinos with fixed energies and incoming angles reaching IceCube. For up-going neutrinos we can clearly see the effects of attenuation in the number of neutrinos arriving with lower energies. The number of ν_τ that reach the detector are greater compared to other flavors due to ν_τ regeneration. We also notice a dip in the number of $\bar{\nu}_e$ at the Glashow resonance $E \simeq 6.3 \times 10^6$ GeV. For down-going neutrinos there is no significant attenuation.

For a flux of cosmogenic neutrinos at Earth $\Phi_{\nu_\alpha}^{\text{Earth}}$ computed using equations (3.3.1) and (3.1.6) for chosen values of the νSI parameters $(m_1, \mathbf{G}_{\text{flav}}, m_\phi)$, we propagated each neutrino species $(\nu_e, \nu_\mu, \nu_\tau, \bar{\nu}_e, \bar{\nu}_\mu, \bar{\nu}_\tau)$ separately through Earth using NuPropEarth to compute the neutrino flux $\Phi_{\nu_\alpha}^{\text{det}}$ reaching IceCube-Gen2 .

Figure 18 shows a flux of cosmogenic neutrinos with and without νSI arriving at IceCube of both down-going and up-going neutrinos. In the low energy range $E_\nu \sim 10^5$ GeV there is no attenuation of the flux. For the case of down-going neutrinos

---

[1] Lookup tables of the transition probabilities generated by Victor Valera
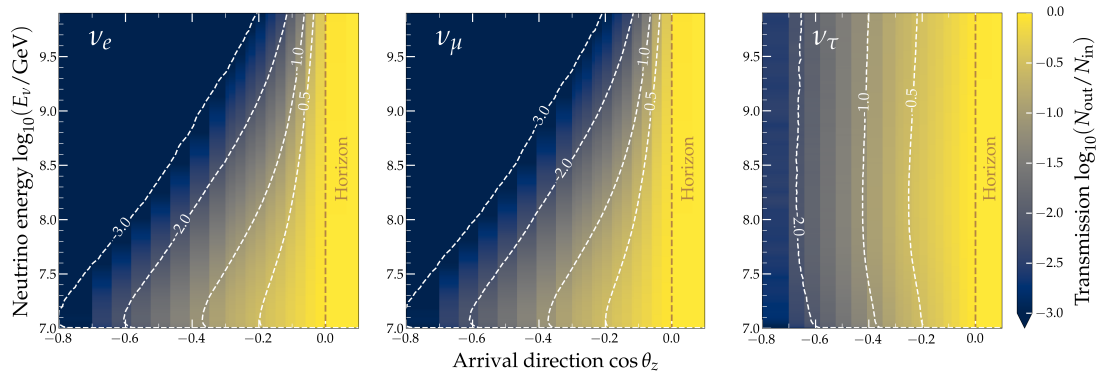

Figure 16: Heatmaps showing the transition probability for cosmogenic ν_e, ν_μ and ν_τ arriving at IceCube as a function of incoming energy and incoming angle. Each data point is generated by injecting a number of neutrinos N_{in} of a fixed energy and incoming angle, then count how many neutrinos N_{out} will arrive at the detector with UHEs ($E_\nu > 10^9$ GeV) and taking the ratio. The dashed lines are isocontours of the transmission probability.

passing through Earth there significant attenuation at UHEs by a few orders of magnitude. The pileup of $\bar{\nu}_e$ below the second νSI resonance $E_2 \sim 2 \times 10^7$ GeV from equation (2.4.5) is shrunk at the Glashow resonance that creates an additional dip in the spectrum. For the flux of ν_τ we see clear effects of ν_τ regeneration, especially around third νSI resonance $E_3 \sim 3 \times 10^6$ GeV, where the corresponding dip in the flux gets elevated due scattering of ν_τ down to lower energies.
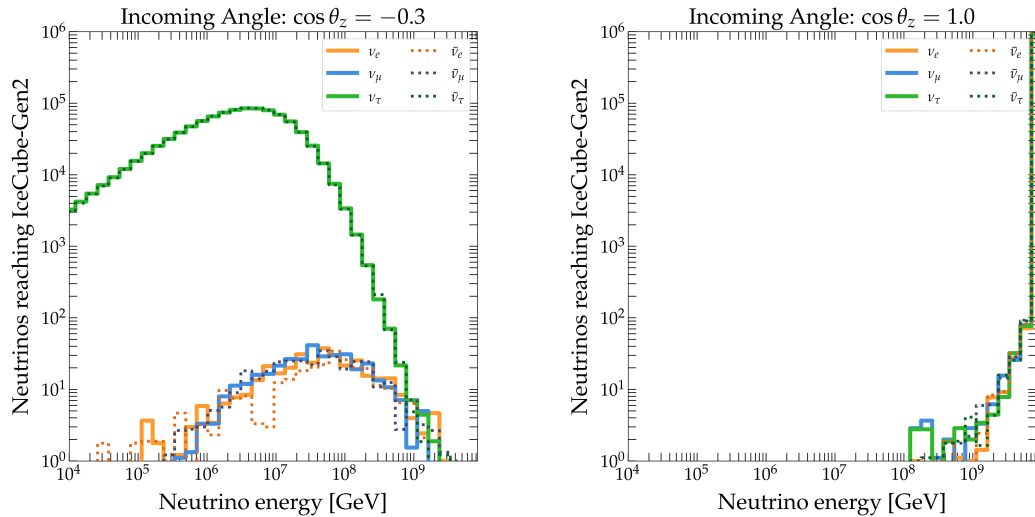
Figure 17: Histogram showing the attenuation of UHE neutrinos traveling through Earth en route to IceCube-Gen2. For each species, $N = 10^6$ neutrinos with energy $E_\nu = 8 \times 10^9$ GeV are injected at a fixed incoming angle θ_z. The number of neutrinos reaching IceCube-Gen2 falling into each energy bin are then counted.
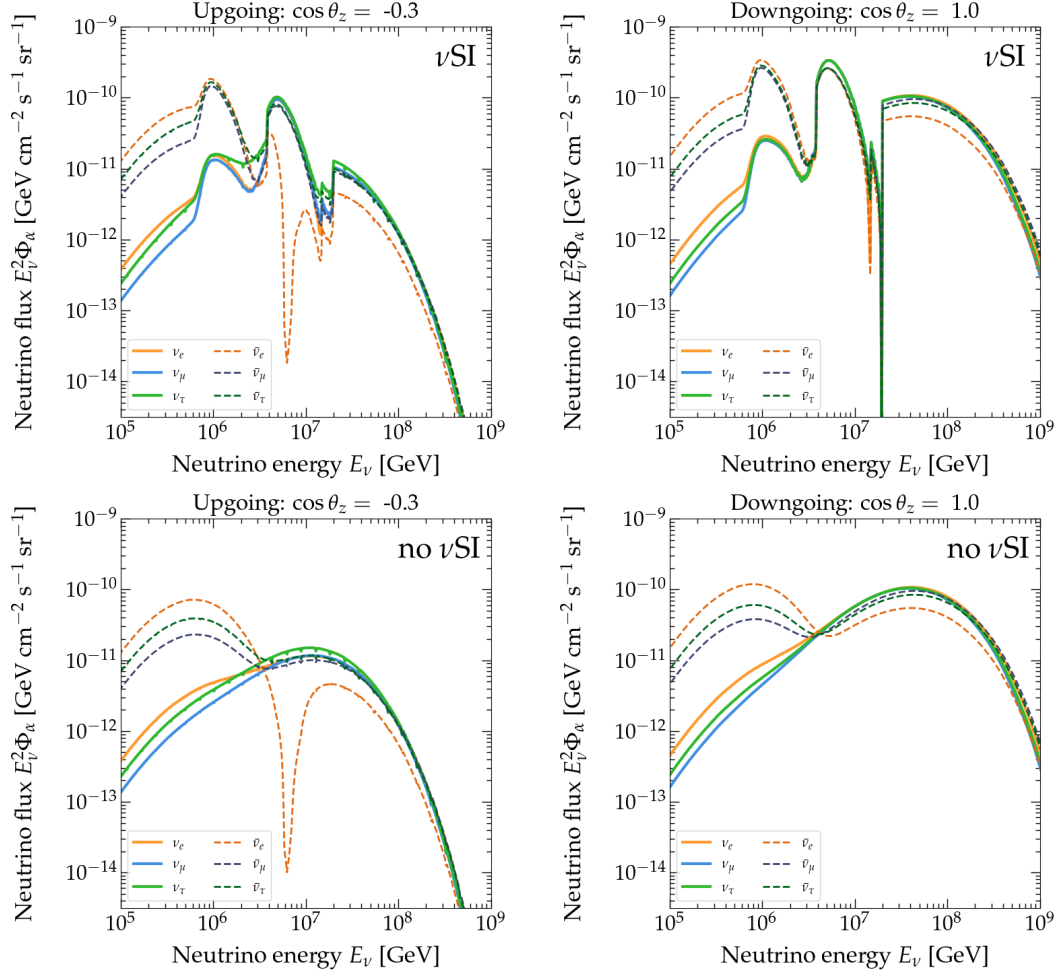
Figure 18: Attenuated fluxes of cosmogenic neutrinos arriving at IceCube after having traversed through the Earth at different incoming angles θ_z. The fluxes in the top panels were Generated assuming $z_{max} = 4$, a mediator mass $m_\phi = 1.07 \times 10^7$ eV, $m_1 = 9.92 \times 10^{-3}$ eV under normal mass ordering, and coupling scenario 1 with $g_{\alpha\alpha} = 9.62 \times 10^{-3}$. The fluxes in the bottom panels were generated without the presence of νSI.

Having discussed the detector properties of IceCube-Gen2 we are now interested in the actual physical observables that allows to make conclusions about the shape of the observed cosmogenic neutrino flux.

For a flux $\Phi_{\nu_\alpha}^{\text{det}}$ of cosmogenic neutrinos arriving at IceCube, the number of events picked up by the detector per energy E_ν, per incoming angle θ_z is given by:

$$\frac{d^2 N_{\nu_\alpha}^i}{dE_\nu d\cos\theta_z} = 2\pi T N_{\text{Av}} \frac{\rho_{\text{ice}}}{m_{\text{ice}}} V_{\text{eff},\nu_\alpha}^i(E_\nu)\sigma_{\nu N}^i(E_\nu)\Phi_{\nu_\alpha}^{\text{det}}(E_\nu,\cos\theta_z)\,, \quad (4.3.1)$$

where the index i indicates either NC or CC contributions. Here N_{Av} is Avogadro's number, $\sigma_{\nu N}^{\text{CC}}(E_\nu)$ is the neutrino-nucleon cross section, ρ_{ice} is the density of ice, m_{ice} is the molar mass of ice, and $V_{\text{eff},\nu_\alpha}^i$ represents the effective volume of the detector. Equation (4.3.1) also holds for anti-neutrinos by replacing $\nu_\alpha \to \bar{\nu}_\alpha$.

Figure 19 shows the computed effective volumes $V_{\text{eff},\nu_\alpha}^i$ for IceCube-Gen2. The effective volume $V_{\text{eff},\nu_\alpha}^i$ describes the detector response to detecting neutrinos of different flavors, as a function of neutrino energy, and averaged over incoming direction. For the effective volume of the upcoming radio array in IceCube-Gen2 we use the models from Ref. [64].

For IceCube-Gen2, CC interactions are the dominant contribution to the event rate, because they produce charged leptons that induce showers with stronger Askaryan emission.

To account for both the energy and angular resolution of IceCube-Gen2, we compute the event spectrum in terms of measurable quantities: The deposited shower energy, E_{dep}, and the reconstructed shower direction, $\theta_{z,\text{rec}}$. A more detailed explanation of how this is done can be found in Appendix B. Thus the detection rate summed over all neutrinos in terms of E_{dep} and $\theta_{z,\text{rec}}$ becomes

$$\frac{d^2 N_\nu}{dE_{\text{dep}}d\cos\theta_{z,\text{rec}}} = \sum_{i=\text{NC,CC}} \sum_{\alpha=e,\mu,\tau} \left(\frac{d^2 N_{\nu_\alpha}^i}{dE_{\text{dep}}d\cos\theta_{z,\text{rec}}} + \frac{d^2 N_{\bar{\nu}_\alpha}^i}{dE_{\text{dep}}d\cos\theta_{z,\text{rec}}} \right)\,. \quad (4.3.2)$$

Hence, the number of detected events in the interval of $[E_{\text{dep}}^{\min}, E_{\text{dep}}^{\max}]$ is

$$N(m_1, \mathbf{G}_{\text{flav}}, m_\phi) = \int_{E_{\text{dep}}^{\min}}^{E_{\text{dep}}^{\max}} dE_{\text{dep}} \int_{-1}^{+1} d\cos\theta_{z,\text{rec}} \left(\frac{d^2 N_\nu(m_1, \mathbf{G}_{\text{flav}}, m_\phi)}{dE_{\text{dep}}d\cos\theta_{z,\text{rec}}} \right)\,. \quad (4.3.3)$$

Figure 20 shows a histogram of the expected number of detected neutrinos at IceCube-Gen2 computed using equation (4.3.3) after $T = 10$ years of exposure time, for different fluxes of cosmogenic neutrinos with and without νSI. The event rates have been multiplied by an artificial factor of $\times 30$ to mimic what one would expect from a flux with a higher normalization, chosen to saturate the current flux limits set by IceCube as seen in Fig. 9. The same flux appearing top panel of Fig. 18 was used to compute the event rate corresponding to the νSI base reference. From Fig. 19 we see that for neutrino energies 10^5–10^7 GeV the effective volume of IceCube-Gen2 is

very low, which makes it difficult to deduce any spectral features that might appear at these energies due to νSI. We can however see a slight reduction in the number events at the highest νSI energy resonance $E_1 \simeq 3 \times 10^7$ GeV and a corresponding pileup at lower energies. Increasing the strength of νSI of the base reference does not have any significant effect on the expected number of events. Decreasing the mediator mass m_ϕ of the base reference will shift the location of the νSI resonances to lower energies by a factor of about $\sim 10^{2.6}$ GeV. This makes them appear at energies where IceCube-Gen2 has poor sensitivity, and there is no difference in the number of expected events compared to the case of no νSI. Increasing the mediator mass m_ϕ with respect to the base reference will shift the pileup neutrinos below lowest νSI resonance E_3 so it appears in the energy range of 10^7–10^8 GeV, as can be seen in Figure 21 of Appendix C. In this scenario there is a pileup of neutrinos in the energy range where the detector seems to be most sensitive, resulting in a significant increase in the expected number of events.
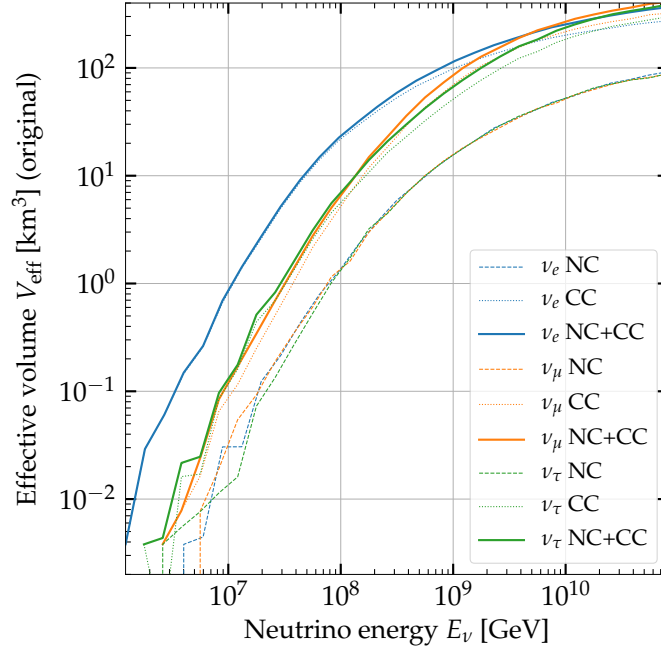

Figure 19: Computed effective volume $V^i_{\mathrm{eff},\nu_\alpha}$ of IceCube-Gen2 for both NC and CC interactions for all neutrino flavors.
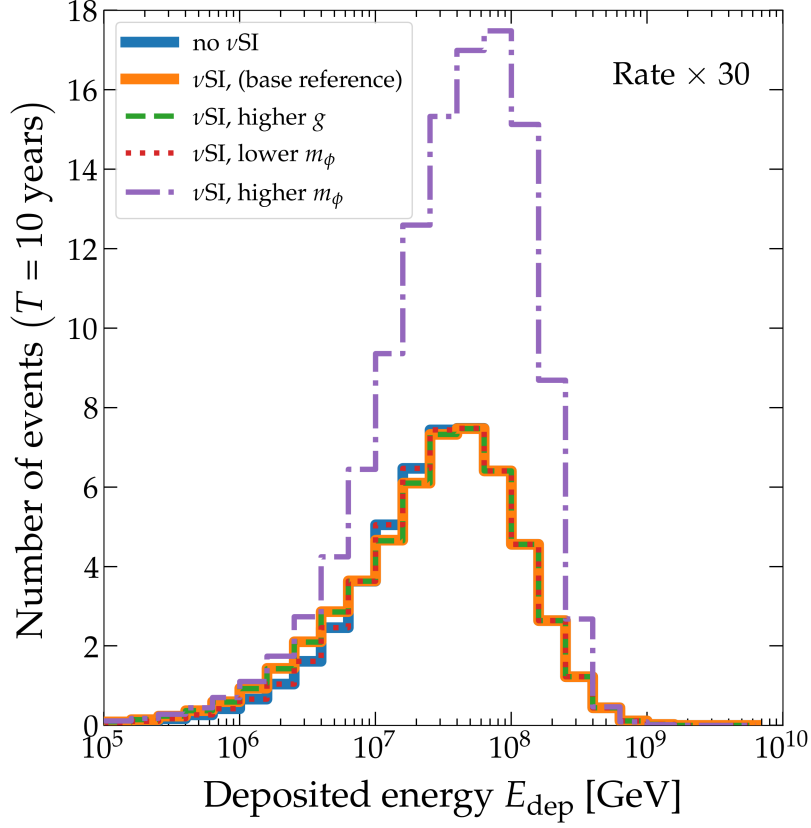
Figure 20: Expected number of events detected at IceCube-Gen2 after 10 years of exposure time for different fluxes of cosmogenic neutrinos as a function of deposited energy. The event rates have been multiplied by an artificial factor of ×30 to mimic what one would expect from a flux with a higher normalization, chosen to saturate the current flux limits set by IceCube as seen in figure 9. The event rate shown by the thick orange line corresponds to a cosmogenic neutrino flux generated assuming $z_{\mathrm{max}} = 4$, a mediator mass $m_\phi = 1.07 \times 10^7$ eV, $m_1 = 9.92 \times 10^{-3}$ eV with normal mass ordering, and scenario 1 with $g_{\alpha\alpha} = 9.62 \times 10^{-3}$. The event rate shown by the green dashed line corresponds to a cosmogenic neutrino flux generated using the same values of the νSI parameters as the orangle line, except for an increased $g_{\alpha\alpha} = 10^{-1}$. The event rate shown by the red dotted line corresponds to a cosmogenic neutrino flux generated using the same values of the νSI parameters as the orange line, except for smaller mediator mass $m_\phi = 10^6$ eV. The event rate shown by the purple dash-dotted line corresponds to a cosmogenic neutrino flux generated using the same values of the νSI parameters as the orange line, except for higher mediator mass $m_\phi = 10^8$ eV.

CONCLUSIONS AND OUTLOOK

In chapter 3 we explored how a flux of cosmogenic neutrinos would respond to variations in each of the individual νSI parameters ($\mathbf{m}_\nu, \mathbf{G}, m_\phi$). We established some general properties of νSI, such as induced dips and pileups in the flux around resonance energies corresponding to each of the three neutrino masses, and how varying the νSI parameters affects their location and amplitude. We also explored how a non-zero νSI coupling between different neutrino mass eigenstates could give rise to stronger or weaker interactions between different neutrino flavors.

In chapter 4 we computed expected number of detected neutrino events by IceCube-Gen2 for a few illustrative fluxes of cosmogenic neutrinos after an exposure time of $T = 10$ years, both with and without νSI as seen in Figure 20. We saw little difference in the number of events computed using our reference flux of selected νSI parameters compared to the case without νSI. This was expected since there is little difference in the amplitude of our reference flux with and without νSI in the energy range of 10^7–10^8 GeV where IceCube-Gen2 seems to the most sensitive. The location of the induced νSI dips/pileups on the cosmogenic neutrino flux relative to energy window of the detector and their amplitude compared to a flux without any νSI are crucial factors when assessing the sensitivity to nuSI..

A similar analysis to ours was recently conducted [41], which focused on detection via the optical component of IceCube-Gen2, rather than the radio component. The optical component will be sensitive to energies of up to only a few tens of PeV. They make use of more sophisticated models for νSI, including more than just the leading interaction terms. They point out some oversights in previous νSI literature, where common approximations such as the δ-function treatment of the s-channel cross-section become unjustifiable in some important cases. They use a simpler model for the production rate of cosmogenic neutrinos, following a power-law with a spectral index and a source density following the star formation rate.

There are current plans aiming to expand upon the work shown in this thesis. A followup paper is in the making that will include a thorough statistical analysis on a broad region of the νSI parameter space. For this we have generated cosmogenic neutrino fluxes reaching IceCube-Gen2 for close to 20×10^6 different configurations of the νSI parameters including inverted mass ordering. This will allow us to systematically explore the νSI parameter space and do statistics on which values of the parameters IceCube-Gen2 might be particularly sensitive to νSI. Future work could involve making use of the NUSIPROP [65] propagation code that was released publicly alongside the paper from Ref. [41] to propagate cosmogenic neutrinos using our computed injection rates from PRINCE and compute fluxes at the detector using the same through earth attenuation treatment with NUPROPEARTH as shown here.

APPENDIX A

A full expansion of equation 3.1.1 for the neutrino flux Φ_i and the included terms that appear within it follow the formalism from Ref. [45].

$$\Phi_i(z, E; m_\phi, \mathbf{G}, \mathbf{m}_\nu) = \frac{1}{1+z} \int_z^\infty \frac{dz'}{H(z')} e^{-\tau_i(z', z, E)} \tilde{S}_i\left[z', \left(\frac{1+z'}{1+z}\right)E\right],$$

$$\tau_i(z', z, E; m_\phi, \mathbf{G}, \mathbf{m}_\nu) = \sum_j \tau_R^{ij}(z, E) \Theta\left[z_{R,j}(z, E) - z\right] \Theta\left[z' - z_{R_j}(z, E)\right],$$

$$\tau_R^{ij}(z, E; m_\phi, \mathbf{G}, m_{\tau,j}) = \frac{\Gamma_R^{ij}(z_{R,j}(z, E))}{H(z_{R,j}(z, E))} \frac{1+z}{1+z_{R,j}(z, E)},$$

$$\tilde{S}_i(z, E; m_\phi, \mathbf{G}) = S_i(z, E) + \sum_{jkl}(1 + \delta_{il})\Gamma_R^{jkil}\Phi_R^{jk}(z, E)\Theta(E_k - E),$$

$$\Gamma_R^{jkil}(z; m_\phi, \mathbf{G}) = n_k(z)\sigma_R^{jkil},$$

$$\Gamma_R^{jk}(z; m_\phi, \mathbf{G}) = \sum_{il}\Gamma_R^{jkil}(z),$$

$$z_{R,i}(z, E; m_\phi, m_{\nu,i}) = (1+z)E_i/E - 1,$$

$$\Phi_R^{ij}(z, E; m, \mathbf{G}, m_{\nu,j}) = \frac{H(z)}{\Gamma_R^{ij}(z)(1+z)} \int_z^\infty \frac{dz'}{H(z')} e^{-\tau_i(z', z, E)}\left[1 - e^{-\tau_R^{ij}(z, E)}\right]\tilde{S}_i\left[z', \frac{(1+z')}{(1+z)}E_{R,j}\right].$$

$$(A.0.1)$$

APPENDIX B

We can rewrite the detection rate in equation 4.3.1 in terms of the measurable quantities E_{dep} and $\theta_{z,\text{rec}}$ as

$$\frac{d^2 N^i_{\nu_\alpha}}{dE_{\text{dep}} d\cos\theta_{z,\text{rec}}} = \int_{-1}^{+1} d\cos\theta_z \int dE_\nu \int dE_{\text{true}} \left[\frac{d^2 N^i_{\nu_\alpha}}{dE_\nu d\cos\theta_z} \cdots \right.$$
$$\left. \cdots R_{E_{\text{true}}}(E_{\text{true}}, E_\nu) R_{E_{\text{dep}}}(E_{\text{dep}}, E_{\text{true}}, E_\nu) R_{\theta_z}(\cos\theta_{z,\text{rec}}, \cos\theta_z) \right] .$$
$$(B.0.1)$$

Here E_{true} is the true energy of the neutrino-initiated shower. $R_{E_{\text{true}}}$, $R_{E_{\text{dep}}}$ and R_{θ_z} are Gaussian envelopes serving as energy and angular resolution functions:

$$R_{E_{\text{true}}}(E_{\text{true}}, E_\nu) = \frac{1}{\sqrt{2\pi\sigma^2_{E_{\text{true}}}(E_\nu)}} \exp\left[-\frac{(E_{\text{true}} - E_{\text{true}}(E_\nu))^2}{2\sigma^2_{E_{\text{true}}}(E_\nu)} \right] , \quad (B.0.2)$$

$$R_{E_{\text{dep}}}(E_{\text{dep}}, E_{\text{true}}, E_\nu) = \frac{1}{\sqrt{2\pi\sigma^2_{E_{\text{dep}}}(E_\nu)}} \exp\left[-\frac{(E_{\text{dep}} - E_{\text{true}})^2}{2\sigma^2_{E_{\text{dep}}}(E_\nu)} \right] , \quad (B.0.3)$$

$$R_\theta(\cos\theta_{z,\text{rec}}, \cos\theta_z) = \frac{1}{\sqrt{2\pi\sigma^2_{\cos\theta_z}(E_\nu)}} \exp\left[-\frac{(\cos\theta_{z,\text{rec}} - \cos\theta_z)^2}{2\sigma^2_{\cos\theta_z}} \right] . \quad (B.0.4)$$

APPENDIX C

Supplemental plots to help better interpret the results from Fig. 20.

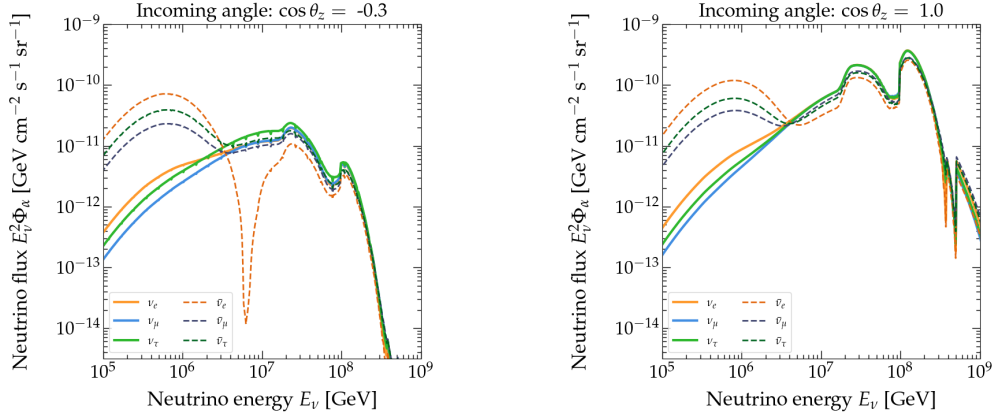

Figure 21: Attenuated fluxes of cosmogenic neutrinos arriving at IceCube after having traversed through the earth at different incoming angles θ_z. Generated assuming $z_{\text{max}} = 4$, a mediator mass $m_\phi = 10^8$ eV, $m_1 = 9.92 \times 10^{-3}$ eV under normal mass ordering, and coupling scenario 1 with $g_{\alpha\alpha} = 9.62 \times 10^{-3}$.

[1] Miguel Escudero and Samuel J. Witte. A cmb search for the neutrino mass mechanism and its relation to the hubble tension. The European Physical Journal C, 80(4), Apr 2020. ISSN 1434-6052. doi: 10.1140/epjc/s10052-020-7854-5. URL http://dx.doi.org/10.1140/epjc/s10052-020-7854-5.

[2] Francis-Yan Cyr-Racine and Kris Sigurdson. Limits on neutrino-neutrino scattering in the early universe. Physical Review D, 90(12), Dec 2014. ISSN 1550-2368. doi: 10.1103/physrevd.90.123533. URL http://dx.doi.org/10.1103/PhysRevD.90.123533.

[3] Maria Archidiacono and Steen Hannestad. Updated constraints on non-standard neutrino interactions from planck. Journal of Cosmology and Astroparticle Physics, 2014(07):046–046, Jul 2014. ISSN 1475-7516. doi: 10.1088/1475-7516/2014/07/046. URL http://dx.doi.org/10.1088/1475-7516/2014/07/046.

[4] Francesco Forastieri, Massimiliano Lattanzi, and Paolo Natoli. Constraints on secret neutrino interactions after planck. Journal of Cosmology and Astroparticle Physics, 2015(07):014–014, Jul 2015. ISSN 1475-7516. doi: 10.1088/1475-7516/2015/07/014. URL http://dx.doi.org/10.1088/1475-7516/2015/07/014.

[5] Isabel M. Oldengott, Thomas Tram, Cornelius Rampf, and Yvonne Y.Y. Wong. Interacting neutrinos in cosmology: exact description and constraints. Journal of Cosmology and Astroparticle Physics, 2017(11):027–027, Nov 2017. ISSN 1475-7516. doi: 10.1088/1475-7516/2017/11/027. URL http://dx.doi.org/10.1088/1475-7516/2017/11/027.

[6] Björn Ahlgren, Tommy Ohlsson, and Shun Zhou. Comment on "is dark matter with long-range interactions a solution to all small-scale problems ofcold dark matter cosmology?". Physical Review Letters, 111(19), Nov 2013. ISSN 1079-7114. doi: 10.1103/physrevlett.111.199001. URL http://dx.doi.org/10.1103/PhysRevLett.111.199001.

[7] Guo-yuan Huang, Tommy Ohlsson, and Shun Zhou. Observational constraints on secret neutrino interactions from big bang nucleosynthesis. Physical Review D, 97(7), Apr 2018. ISSN 2470-0029. doi: 10.1103/physrevd.97.075009. URL http://dx.doi.org/10.1103/PhysRevD.97.075009.

[8] Nikita Blinov, Kevin J. Kelly, Gordan Krnjaic, and Samuel D. McDermott. Constraining the self-interacting neutrino interpretation of the hubble tension. Physical Review Letters, 123(19), Nov 2019. ISSN 1079-7114. doi: 10.1103/physrevlett.123.191102. URL http://dx.doi.org/10.1103/PhysRevLett.123.191102.

[9] Edward W. Kolb and Michael S. Turner. Supernova 1987a and the secret interactions of neutrinos. Phys. Rev. D, 36:2895–2900, Nov 1987. doi: 10.1103/PhysRevD.36.2895. URL https://link.aps.org/doi/10.1103/PhysRevD.36.2895.

[10] Shashank Shalgar, Irene Tamborra, and Mauricio Bustamante. Core-collapse supernovae stymie secret neutrino interactions. Physical Review D, 103(12), Jun 2021. ISSN 2470-0029. doi: 10.1103/physrevd.103.123008. URL http://dx.doi.org/10.1103/PhysRevD.103.123008.

[11] Mikhail S. Bilenky and Arcadi Santamaria. 'Secret' neutrino interactions. In Neutrino Mixing: Meeting in Honor of Samoil Bilenky's 70th Birthday, 8 1999.

[12] A. P. Lessa and O. L. G. Peres. Revising limits on neutrino-majoron couplings. Physical Review D, 75(9), May 2007. ISSN 1550-2368. doi: 10.1103/physrevd.75.094001. URL http://dx.doi.org/10.1103/PhysRevD.75.094001.

[13] Ranjan Laha, Basudeb Dasgupta, and John F. Beacom. Constraints on new neutrino interactions via light abelian vector bosons. Physical Review D, 89 (9), May 2014. ISSN 1550-2368. doi: 10.1103/physrevd.89.093025. URL http://dx.doi.org/10.1103/PhysRevD.89.093025.

[14] Jeffrey M. Berryman, André de Gouvêa, Kevin J. Kelly, and Yue Zhang. Lepton-number-charged scalars and neutrino beamstrahlung. Physical Review D, 97 (7), Apr 2018. ISSN 2470-0029. doi: 10.1103/physrevd.97.075030. URL http://dx.doi.org/10.1103/PhysRevD.97.075030.

[15] Kevin J. Kelly and Pedro A.N. Machado. Multimessenger astronomy and new neutrino physics. Journal of Cosmology and Astroparticle Physics, 2018(10): 048–048, Oct 2018. ISSN 1475-7516. doi: 10.1088/1475-7516/2018/10/048. URL http://dx.doi.org/10.1088/1475-7516/2018/10/048.

[16] Mauricio Bustamante, Charlotte Rosenstrøm, Shashank Shalgar, and Irene Tamborra. Bounds on secret neutrino interactions from high-energy astrophysical neutrinos. Physical Review D, 101(12), Jun 2020. ISSN 2470-0029. doi: 10.1103/physrevd.101.123024. URL http://dx.doi.org/10.1103/PhysRevD.101.123024.

[17] V. S. Berezinsky and G. T. Zatsepin. Cosmic rays at ultrahigh-energies (neutrino?). Phys. Lett. B, 28:423–424, 1969. doi: 10.1016/0370-2693(69)90341-4.

[18] Ellis Charles Drummond and Wooster W. A. The average energy of disintegration of radium e. Proc. R. Soc. Lond., (A117109–123), 1927. URL http://doi.org/10.1098/rspa.1927.0168.

[19] John N. Bahcall. Solar neutrinos. i. theoretical. Phys. Rev. Lett., 12:300–302, Mar 1964. doi: 10.1103/PhysRevLett.12.300. URL https://link.aps.org/doi/10.1103/PhysRevLett.12.300.

[20] Raymond Davis. Solar neutrinos. ii. experimental. Phys. Rev. Lett., 12:303–305, Mar 1964. doi: 10.1103/PhysRevLett.12.303. URL https://link.aps.org/doi/10.1103/PhysRevLett.12.303.

[21] Mauricio Bustamante et al. Cosmic Neutrino Probes of Fundamental Physics. Snowmass - Letter of interest, 2021. URL https://www.snowmass21.org/docs/files/summaries/CF/SNOWMASS21-CF7_CF1-NF4_NF3-TF11_TF0_Mauricio_Bustamante-048.pdf.

[22] John N. Bahcall, Aldo M. Serenelli, and Sarbani Basu. New solar opacities, abundances, helioseismology, and neutrino fluxes. The Astrophysical Journal, 621(1):L85–L88, Jan 2005. ISSN 1538-4357. doi: 10.1086/428929. URL http://dx.doi.org/10.1086/428929.

[23] Carlo Giunti and Chung W. Kim. Fundamentals of Neutrino Physics and Astrophysics. 2007. ISBN 978-0-19-850871-7.

[24] Ofelia Pisanti. Astrophysical neutrinos: theory. Journal of Physics: Conference Series, 1263:012004, Jun 2019. ISSN 1742-6596. doi: 10.1088/1742-6596/1263/1/012004. URL http://dx.doi.org/10.1088/1742-6596/1263/1/012004.

[25] Shouvik Roy Choudhury and Sandhya Choubey. Updated bounds on sum of neutrino masses in various cosmological scenarios. Journal of Cosmology and Astroparticle Physics, 2018(09):017–017, Sep 2018. ISSN 1475-7516. doi: 10.1088/1475-7516/2018/09/017. URL http://dx.doi.org/10.1088/1475-7516/2018/09/017.

[26] Ivan Esteban, M.C. Gonzalez-Garcia, Michele Maltoni, Thomas Schwetz, and Albert Zhou. The fate of hints: updated global analysis of three-flavor neutrino oscillations. Journal of High Energy Physics, 2020(9), Sep 2020. ISSN 1029-8479. doi: 10.1007/jhep09(2020)178. URL http://dx.doi.org/10.1007/JHEP09(2020)178.

[27] http://www.nu-fit.org/.

[28] Y. Chikashige, R.N. Mohapatra, and R.D. Peccei. Are there real goldstone bosons associated with broken lepton number? Physics Letters B, 98(4):265–268, 1981. ISSN 0370-2693. doi: https://doi.org/10.1016/0370-2693(81)90011-3. URL https://www.sciencedirect.com/science/article/pii/0370269381900113.

[29] G.B. Gelmini and M. Roncadelli. Left-handed neutrino mass scale and spontaneously broken lepton number. Physics Letters B, 99(5):411–415, 1981. ISSN 0370-2693. doi: https://doi.org/10.1016/0370-2693(81)90559-1. URL https://www.sciencedirect.com/science/article/pii/0370269381905591.

[30] Howard M. Georgi, Sheldon Lee Glashow, and Shmuel Nussinov. Unconventional model of neutrino masses. Nuclear Physics B, 193(2):297–316, 1981. ISSN 0550-3213. doi: https://doi.org/10.1016/0550-3213(81)90336-9. URL https://www.sciencedirect.com/science/article/pii/0550321381903369.

[31] Graciela B. Gelmini, Shmuel Nussinov, and Marco Roncadelli. Bounds and prospects for the majoron model of left-handed neutrino masses. Nuclear Physics B, 209(1):157–173, 1982. ISSN 0550-3213. doi: https://doi.org/10.1016/0550-3213(82)90107-9. URL https://www.sciencedirect.com/science/article/pii/0550321382901079.

[32] Shmuel Nussinov and Marco Roncadelli. Observable effects of relic majorons. Physics Letters B, 122(5):387–391, 1983. ISSN 0370-2693. doi: https://doi.org/10.1016/0370-2693(83)91588-5. URL https://www.sciencedirect.com/science/article/pii/0370269383915885.

[33] Kfir Blum, Anson Hook, and Kohta Murase. High energy neutrino telescopes as a probe of the neutrino mass mechanism, 2014.

[34] Takeshi Araki, Fumihiro Kaneko, Yasufumi Konishi, Toshihiko Ota, Joe Sato, and Takashi Shimomura. Cosmic neutrino spectrum and the muon anomalous magnetic moment in the gaugedllmodel. Physical Review D, 91(3), Feb 2015. ISSN 1550-2368. doi: 10.1103/physrevd.91.037301. URL http://dx.doi.org/10.1103/PhysRevD.91.037301.

[35] Takeshi Araki, Fumihiro Kaneko, Toshihiko Ota, Joe Sato, and Takashi Shimomura. Mev scale leptonic force for cosmic neutrino spectrum and muon anomalous magnetic moment. Physical Review D, 93(1), Jan 2016. ISSN 2470-0029. doi: 10.1103/physrevd.93.013014. URL http://dx.doi.org/10.1103/PhysRevD.93.013014.

[36] Laura G. van den Aarssen, Torsten Bringmann, and Christoph Pfrommer. Is dark matter with long-range interactions a solution to all small-scale problems ofcold dark matter cosmology? Physical Review Letters, 109(23), Dec 2012. ISSN 1079-7114. doi: 10.1103/physrevlett.109.231301. URL http://dx.doi.org/10.1103/PhysRevLett.109.231301.

[37] John F. Cherry, Alexander Friedland, and Ian M. Shoemaker. Neutrino portal dark matter: From dwarf galaxies to icecube, 2014.

[38] Gabriela Barenboim, Peter B. Denton, and Isabel M. Oldengott. Constraints on inflation with an extended neutrino sector. Physical Review D, 99(8), Apr 2019. ISSN 2470-0029. doi: 10.1103/physrevd.99.083515. URL http://dx.doi.org/10.1103/PhysRevD.99.083515.

[39] B. J. P. Jones and J. Spitz. Neutrino flavor transformations from new short-range forces, 2019.

[40] M G Aartsen, R Abbasi, M Ackermann, J Adams, J A Aguilar, M Ahlers, M Ahrens, C Alispach, P Allison, N M Amin, and et al. Icecube-gen2: the window to the extreme universe. Journal of Physics G: Nuclear and Particle Physics, 48(6):060501, Apr 2021. ISSN 1361-6471. doi: 10.1088/1361-6471/abbd48. URL http://dx.doi.org/10.1088/1361-6471/abbd48.

[41] Ivan Esteban, Sujata Pandey, Vedran Brdar, and John F. Beacom. Probing secret interactions of astrophysical neutrinos in the high-statistics era, 2021.

[42] Yvonne Y.Y. Wong. Neutrino mass in cosmology: Status and prospects. Annual Review of Nuclear and Particle Science, 61(1):69–98, 2011. doi: 10.1146/annurev-nucl-102010-130252. URL https://doi.org/10.1146/annurev-nucl-102010-130252.

[43] Jonas Heinze, Anatoli Fedynitch, Denise Boncioli, and Walter Winter. A new view on auger data and cosmogenic neutrinos in light of different nuclear disintegration and air-shower models. The Astrophysical Journal, 873(1):88, Mar 2019. ISSN 1538-4357. doi: 10.3847/1538-4357/ab05ce. URL http://dx.doi.org/10.3847/1538-4357/ab05ce.

[44] Marc, Bryan Weinstein, tgwoodcock, Cory Simon, chebee7i, Wiley Morgan, Vince Knight, Nick Swanson-Hysell, Matthew Evans, jl bernal, ZGainsforth, The Gitter Badger, SaxonAnglo, Maximiliano Greco, and Guido Zuidhof. marcharper/python-ternary: Version 1.0.6, April 2019. URL https://doi.org/10.5281/zenodo.2628066.

[45] Cyril Creque-Sarbinowski, Jeffrey Hyde, and Marc Kamionkowski. Resonant neutrino self-interactions. Physical Review D, 103(2), Jan 2021. ISSN 2470-0029. doi: 10.1103/physrevd.103.023527. URL http://dx.doi.org/10.1103/PhysRevD.103.023527.

[46] Particle Data Group. Review of Particle Physics. Progress of Theoretical and Experimental Physics, 2020(8), 08 2020. ISSN 2050-3911. doi: 10.1093/ptep/ptaa104. URL https://doi.org/10.1093/ptep/ptaa104. 083C01.

[47] Jonas Heinze and Anatoli Fedynitch. https://github.com/joheinze/PriNCe, 2020. PriNCe.

[48] Francesco Fenu. The cosmic ray energy spectrum measured using the Pierre Auger Observatory. PoS, ICRC2017:486, 2018. doi: 10.22323/1.301.0486.

[49] Jose Bellido. Depth of maximum of air-shower profiles at the Pierre Auger Observatory: Measurements above $10^{17.2}$ eV and Composition Implications. PoS, ICRC2017:506, 2018. doi: 10.22323/1.301.0506.

[50] M. Kachelrieß, E. Parizot, and D. V. Semikoz. The gzk horizon and constraints on the cosmic ray source spectrum from observations in the gzk regime. JETP Letters, 88(9):553–557, Jan 2009. ISSN 1090-6487. doi: 10.1134/s0021364008210017. URL http://dx.doi.org/10.1134/S0021364008210017.

[51] R. Abbasi, M. Ackermann, J. Adams, J.A. Aguilar, M. Ahlers, M. Ahrens, C. Alispach, A.A. Alves, N.M. Amin, K. Andeen, and et al. Icecube high-energy starting event sample: Description and flux characterization with 7.5 years of data. Physical Review D, 104(2), Jul 2021. ISSN 2470-0029. doi: 10.1103/physrevd.104.022002. URL http://dx.doi.org/10.1103/PhysRevD.104.022002.

[52] M.G. Aartsen, M. Ackermann, J. Adams, J.A. Aguilar, M. Ahlers, M. Ahrens, I. Al Samarai, D. Altmann, K. Andeen, T. Anderson, and et al. Differential limit on the extremely-high-energy cosmic neutrino flux in the presence of astrophysical background from nine years of icecube data. Physical Review D, 98(6), Sep 2018. ISSN 2470-0029. doi: 10.1103/physrevd.98.062003. URL http://dx.doi.org/10.1103/PhysRevD.98.062003.

[53] Markus Ahlers, Klaus Helbing, and Carlos Pérez de los Heros. Probing particle physics with icecube. The European Physical Journal C, 78(11), Nov 2018. ISSN 1434-6052. doi: 10.1140/epjc/s10052-018-6369-9. URL http://dx.doi.org/10.1140/epjc/s10052-018-6369-9.

[54] Stefan Schönert, Thomas K. Gaisser, Elisa Resconi, and Olaf Schulz. Vetoing atmospheric neutrinos in a high energy neutrino telescope. Physical Review D, 79(4), Feb 2009. ISSN 1550-2368. doi: 10.1103/physrevd.79.043009. URL http://dx.doi.org/10.1103/PhysRevD.79.043009.

[55] Thomas K. Gaisser, Kyle Jero, Albrecht Karle, and Jakob van Santen. Generalized self-veto probability for atmospheric neutrinos. Physical Review D, 90(2), Jul 2014. ISSN 1550-2368. doi: 10.1103/physrevd.90.023009. URL http://dx.doi.org/10.1103/PhysRevD.90.023009.

[56] G. A. Askar'yan. Excess negative charge of an electron-photon shower and its coherent radio emission. Zh. Eksp. Teor. Fiz., 41:616–618, 1961.

[57] J. Alvarez-Muñiz and E. Zas. The lpm effect for eev hadronic showers in ice: implications for radio detection of neutrinos. Physics Letters B, 434(3-4): 396–406, Aug 1998. ISSN 0370-2693. doi: 10.1016/s0370-2693(98)00905-8. URL http://dx.doi.org/10.1016/S0370-2693(98)00905-8.

[58] Alfonso Garcia, Rhorry Gauld, Aart Heijboer, and Juan Rojo. Complete predictions for high-energy neutrino propagation in matter. Journal of Cosmology and Astroparticle Physics, 2020(09):025–025, Sep 2020. ISSN 1475-7516. doi: 10.1088/1475-7516/2020/09/025. URL http://dx.doi.org/10.1088/1475-7516/2020/09/025.

[59] Amanda Cooper-Sarkar, Philipp Mertsch, and Subir Sarkar. The high energy neutrino cross-section in the standard model and its uncertainty. Journal of High Energy Physics, 2011(8), Aug 2011. ISSN 1029-8479. doi: 10.1007/jhep08(2011) 042. URL http://dx.doi.org/10.1007/JHEP08(2011)042.

[60] Raj Gandhi, Chris Quigg, Mary Hall Reno, and Ina Sarcevic. Neutrino interactions at ultrahigh energies. Physical Review D, 58(9), Sep 1998. ISSN 1089-4918. doi: 10.1103/physrevd.58.093009. URL http://dx.doi.org/10.1103/PhysRevD.58.093009.

[61] Amy Connolly, Robert S. Thorne, and David Waters. Calculation of high energy neutrino-nucleon cross sections and uncertainties using the martinstirling-thorne-watt parton distribution functions and implications for future experiments. Physical Review D, 83(11), Jun 2011. ISSN 1550-2368. doi: 10.1103/physrevd.83.113009. URL http://dx.doi.org/10.1103/PhysRevD.83.113009.

[62] Richard S. Sutton and Brian Tanner. Temporal-difference networks, 2015.

[63] Adam M. Dziewonski and Don L. Anderson. Preliminary reference earth model. Physics of the Earth and Planetary Interiors, 25(4):297–356, 1981. ISSN 0031-9201. doi: https://doi.org/10.1016/0031-9201(81)90046-7. URL https://www.sciencedirect.com/science/article/pii/0031920181900467.

[64] D. García-Fernández, A. Nelles, and C. Glaser. Signatures of secondary leptons in radio-neutrino detectors in ice. Physical Review D, 102(8), Oct 2020. ISSN 2470-0029. doi: 10.1103/physrevd.102.083011. URL http://dx.doi.org/10.1103/PhysRevD.102.083011.

[65] Ivan Esteban, Sujata Pandey, Vedran Brdar, and John F. Beacom. nusiprop. https://github.com/ivan-esteban-phys/nuSIprop, 2021.